J. Fluid Mech. (1995), *vol.* 294, *pp.* 123–154

Interaction dynamics of solitary waves on a falling film

By H.-C. CHANG,† E. DEMEKHIN‡ AND E. KALAIDIN‡

Department of Chemical Engineering, University of Notre Dame, Notre Dame, IN 46556, USA

(Received 26 August 1994 and in revised form 23 February 1995)

Beyond a short transition region near the inlet, waves on a falling film evolve into distinct pulse-like solitary waves that dominate all subsequent interfacial dynamics. Numerical and physical experiments indicate that these localized structures can attract and repel each other. Attractive interaction through the capillary ripples of the pulses causes two pulses to coalesce into a bigger pulse which accelerates and precipitates further coalescence. This binary interaction between an 'excited' pulse after coalescence and its smaller front neighbour is the key mechanism that drives the observed wave dynamics. From symmetry arguments, two dominant modes for a solitary pulse are obtained and used to develop an inelastic coherent structure theory for binary interaction between an excited pulse and its front neighbour. The theory offers a simple dynamical system that quantitatively describes the binary interaction and promises to elucidate the complex wave dynamics on a falling film.

1. Introduction

Unlike many other hydrodynamic systems, the nearly sinusoidal waves at the inception region of a falling film evolve downstream into wave structures with a drastically different shape. The sinusoidal waves trigger their subharmonics and other (sideband) modes and all these harmonics synchronize to form distinct localized pulses or 'humps' which travel steadily at approximately constant speeds over a distance long compared to the pulse width. Unlike the sinusoidal waves, each individual pulse has a broad Fourier content but all the Fourier harmonics are phase-locked. As a result, one cannot study the dynamics of these 'solitary waves' using the classical Ginzburg–Landau-type amplitude formulation which considers only a small band of harmonics near criticality. Liu & Gollub (1993) have recently scrutinized this evolution to solitary waves experimentally and Cheng & Chang (1995) have offered a theoretical classification of the secondary instabilities of the sinusoidal waves which trigger the evolution towards the solitary waves.

These solitary waves will eventually develop transverse variations which pinch off their crests to form crescent-shaped waves called 'scallop waves' and other localized three-dimensional wave structures (Chang *et al.* 1994; Liu & Gollub 1994). However, for a very large region, which is much larger than the sinusoidal wave region and whose domain size increases with increasing inclination angle from vertical,

† Author to whom correspondence should be addressed.
‡ Permanent Address: Department of Applied Mathematics, Kuban State Technological University, Krasnodar, 3500072, Russia.

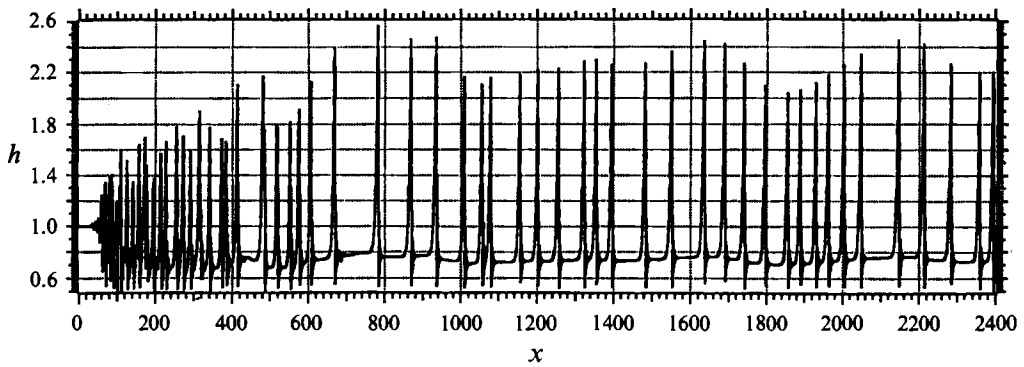

FIGURE 1. Snapshot of the evolving waves from a numerical simulation of the averaged equation at $\delta = 0.217$. Random forcing is placed at the inlet and a 'soft' boundary condition is placed at the exit to minimize upstream feedback from there.

the interfacial dynamics is dominated by interaction among the two-dimensional pulses. In §2, we perform some numerical experiments to clarify the dynamics in this important region and to obtain quantitative characterizations of the dynamics that have not been measured in physical experiments. It will be demonstrated that the pulse dynamics is dominated by a binary interaction which is best explained by a coherent structure theory that is capable of describing the important phenomenon of coalescence. The theory is preceded by an investigation of the spectrum of the solitary pulse in §3 where the dominant modes of the pulses that are excited during the interaction and how they are related to the symmetries of the system are delineated. The full theory is developed in §4 which also offers a quantitative comparison of the theoretical prediction against numerical data to demonstrate the validity of the simple theory to describe pulse interaction dynamics. A discussion on possible extensions is presented in the final §5.

2. Numerical experiments

The evolution from the sinusoidal waves near the inception region to solitary pulses which interact over a very large domain is clearly evident in our numerical simulation shown in figure 1. Unlike earlier studies, a periodic boundary condition is not assumed here. Instead, we have developed a code that can capture the downstream convective nature of the wave evolution. The complete Navier–Stokes equation still escapes the computational capability of our code and we use instead the ad hoc averaged equations, first derived by Shkadov (1967) and known sometimes as the Kapitsa–Shkadov equation, for the vertical film where the velocity profile beneath the film is assumed to be of a parabolic form (see Chang 1994 for a review of this equation)

$$\left.\begin{aligned} \frac{\partial q}{\partial t} + \frac{6}{5}\frac{\partial}{\partial x}(q^2/h) - \frac{1}{5\delta}(hh_{xxx} + h - q/h^2) = 0, \\ \frac{\partial h}{\partial t} + \frac{\partial q}{\partial x} = 0. \end{aligned}\right\} \tag{2.1}$$

The interfacial height is h and the average flow rate is q. The lone parameter δ is a normalized Reynolds or inverse Weber number defined by $\delta = R^{11/9}/5\gamma^{1/3}3^{7/9} = R/15\kappa$ where $R = \langle u\rangle h_N/\nu$ is the Reynolds number based on the average fluid velocity $\langle u\rangle = gh_N^2/3\nu$, h_N is the Nusselt flat-film thickness and ν is the kinematic

viscosity of the fluid. The Kapitza number $\gamma = WR^{5/3}/3^{1/3} = \sigma\nu^{-4/3}g^{-1/3}/\rho$ is only a function of the fluid properties and not a function of the flow rate. The parameter $W = \sigma/\rho\langle u\rangle^2 h_N$ is the Weber number. The parameter κ is a large number defined by $\kappa^3 = WR/3$. In the averaged equation, the downstream velocity is scaled by $\langle u\rangle$ and the interfacial height by h_N. The transverse velocity is, however, scaled by $\langle u\rangle\kappa^{-1}$, the downstream coordinate by $h_N\kappa$ and time by $h_N\kappa/\langle u\rangle$ to reflect the nearly parallel, long-wave and slow evolution character of the wave dynamics. Speed is then scaled by the average fluid velocity $\langle u\rangle$ of a flat film. At low δ, inertia becomes secondary and more rigorous long-wave expansion of the equations of motion at low Reynolds number leads to evolution equations (known sometimes as Benny's equations) that involve only the interfacial height h. The flow rate is removed by a quasi-steady approximation of the flow under the interface. Although these equations are simpler and more rigorous (they also have some limitations, see Chang 1994), we have avoided them here because they do not yield the observed solitary wave solutions at high flow rates (Pumir,Manneville & Pomeau 1983; Chang 1994; Salamon,Armstrong & Brown 1994). Also, as we shall demonstrate subsequently, solitary pulses are unstable to local disturbances at low flow rates and they tend to split up. The solitary wave dynamics at low flow rate (lubrication conditions) is hence quite different from that at higher flow rates. (See numerical studies by Pumir *et al.* 1983 and by Kalliadasis & Chang 1994, for a related problem). The averaged equation is a simple model equation which is believed to reproduce all the pertinent dynamics qualitatively at the high flow rate regimes and even offer some surprising quantitative accuracy for $\delta < 0.1$ (Demekhin, Kaplan & Shkadov 1987). It also reduces to the Kuramoto–Sivashinsky(KS) evolution equation if a long-wave expansion is carried out at low flow rates (Chang, Demekhin & Kopelevich 1993*a*) for vanishingly small δ and wave amplitude,

$$H_\tau + 4HH_\xi + H_{\xi\xi} + H_{\xi\xi\xi\xi} = 0 \tag{2.2}$$

where H, ξ and τ are the scaled interfacial height, downstream position and time, respectively, $H = 3(h-1)/2\alpha_0^3$, $\xi = (x-3t)\alpha_0$ and $\tau = \alpha_0^4 t$. The parameter $\alpha_0 = (18\delta)^{1/2}$ is the neutral wavenumber in the limit of vanishing δ. If the averaged equations (2.1) are used insead of the full equations of motion, the ad hoc parabolic velocity profile yields $\alpha_0 = (15\delta)^{1/2}$. The above scaling is the usual amplitude shrinking, length and time stretching of a weakly nonlinear analysis for the four terms in (2.2) (representing evolution, kinematic nonlinearity, inertial growth and capillary 'dissipation') to balance. We note that, owing to the scaling in ξ and τ, the speed of a stationary solitary pulse $\hat{c}$ of (2.2) is related to the speed c^* of a solitary pulse of (2.1) by $\hat{c} = (c^* - 3)/\alpha_0^3$. Since the parameter δ has been absorbed in the KS equation, a single solitary pulse solution to (2.2) actually represents an entire family of pulses to (2.1) parameterized by δ, as one transforms back to the coordinates of (2.1). Demekhin & Shdadov (1986) and Kawahara & Toh (1988) have shown that the KS equation (2.2) does have a unique single-hump solitary pulse (see also Chang 1986; Chang *et al.* 1993*a*) and hence a one-parameter family of solitary pulse exists for (2.1) in the limit when the KS equation holds. This family will be constructed subsequently and extended beyond the limit of small-amplitude waves of the KS equation. The shape, speed and amplitude of each member of this family differ. However, since the KS scaling for $\hat{c}$ and H are the same with respect to α_0, the ratio $(c^* - 3)/(h_m - 1)$, where $h_m - 1$ is the amplitude of the solitary pulse, should be independent of δ for the family generated by the KS solitary pulse. This remains a good approximation even beyond the KS limit of small-amplitude waves. In fact, Chang,Demekhin & Kopelevich

(1993*b*) showed that $H/\hat{c}$ for the KS solitary wave is about 1.5 and we hence expect $(c^*-3)/(h_m-1)$ of the solitary pulse family of the averaged equation to be about 2.25.

For simplicity, we have considered only the case of a vertically falling film. Averaged equations can also be derived for inclined films (Prokopiou, Cheng & Chang 1991). The inclination angle has the important effect of allowing gravity to stabilize the film. The stabilization occurs at several stages. The primary instability is suppressed by gravity and it requires significantly more inertia to trigger the onset of waves. More specifically, the critical Reynolds number scales as $\tan\theta$ where θ is the inclination angle measured from the vertical. The nonlinear evolution beyond onset is also slowed signficantly because of this gravitational stabilization. For example, the thicker film at onset introduces the gravity–capillary dispersion mechanism of deep water waves and this enhanced dispersion delays the synchronization (phase locking) of the Fourier modes to form solitary waves (Cheng & Chang 1995). Once formed, however, the solitary waves tend to be less susceptible to transverse disturbances. This is because the transverse variation is triggered by a Rayleigh capillary instability at the crest of the solitary pulse and the intensity of this instability is determined by the crest curvature which scales as the inverse of the pulse width. The latter is determined by a balance between capillary smoothing and gravitational steepening. On an inclined plane, the gravitational steepening effect is weaker. The pulse is hence wider and the transverse Rayleigh instability less intense. This is why many solitary wave experiments are carried out on an inclined plane (Liu & Gollub 1994). However, the slower dynamics on an incline also implies that some of the rich solitary wave dynamics described here can only be observed on a very long plane. To reduce computational effort, we have restricted ourselves to a vertically falling film but have also neglected the transverse secondary instability which will eventually destroy the solitary waves (Chang *et al.* 1994).

For a given δ value, we have imposed random forcing at the inlet in figure 1 at $x = 0$, and by $x = 200$ distinct solitary pulses have formed and the thickness of the substrate layer has been considerably reduced relative to the original Nusselt flat film, which has been scaled to unity, at the inlet. Each individual pulse travels in a stationary manner over a distance much larger than the pulse width w (~ 50 units in figure 1) as shown by the'world lines' of figure 2. However, its speed and amplitude do evolve slowly over a length scale far larger than the pulse width. The most dramatic phenomenon, however, is that the solitary pulses can be annihilated when two pulses coalesce to form a single large pulse, as was first observed in Liu & Gollub's (1994) experiments. Two pulses close to coalescence are observed at $x = 380$ in the snapshot of figure 1 and a large pulse formed after a coalescence is seen immediately downstream. These coalescence phenomena are also evident from the world lines in figure 2. It is the coalescence, which converts two pulses into a large one, that causes the average pulse speed, pulse amplitude and separation between pulses to increase downstream. Stainthorp & Allen (1965) and our recent measurements have experimentally confirmed the increase in the average wave velocity. The increase in average amplitude is evident in figure 1 since the mass-carrying pulses become larger as their number diminishes. We have also obtained the average separation at every station from our numerical experiment. The result shown in figure 2 clearly demonstrates a linear increase downstream. Further downstream, however, the average separation approaches an equilibrium value beyond which coalescence ceases to occur and no further increase in the average separation, speed or amplitude is observed.

To further understand this solitary pulse evolution dynamics, we have numerically

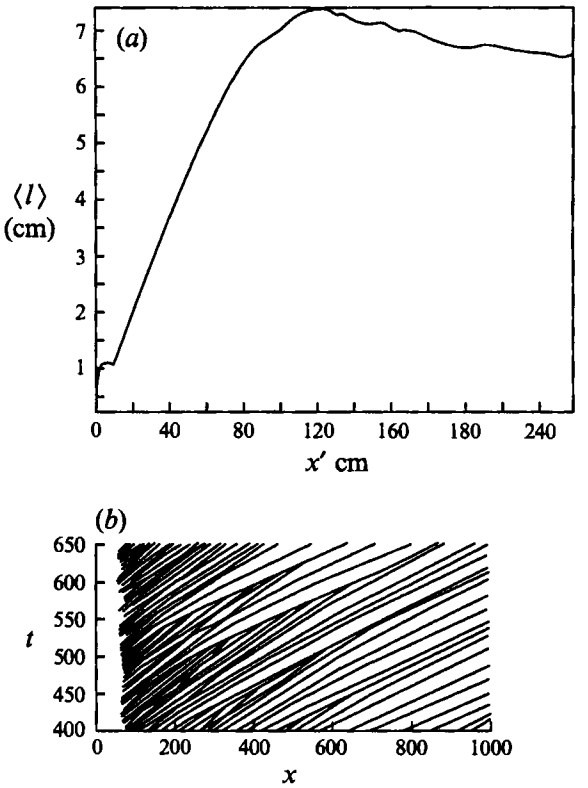

FIGURE 2. (*a*) The average separation between pulses as a function of position in real units for the numerical experiment of figure 1. (*b*) The world lines tracking the pulses of figure 1 in the space (x)–time (t) coordinates of the averaged equation. At $\delta = 0.217$ for water, $\kappa = 6.8, h_N = 0.014$ cm and $\langle u \rangle = 6.5$ cm s^{-1}. This yields a downstream length scale of $\kappa h_N = 0.1$ cm and a time scale of $h_N \kappa / \langle u \rangle = 0.015$ s.

constructed the solitary pulse solution to (1) in the moving frame $x - c^* t$ as shown in figure 3. These solitary pulse solutions approach at infinity the Nusselt flat-film solution, which has been scaled to unity, $h^*(x \to \pm\infty) = 1$, and are described by

$$\left.\begin{aligned} -c\frac{\partial q}{\partial x} + \frac{6}{5}\frac{\partial}{\partial x}(q^2/h) - \frac{1}{5\delta}(hh_{xxx} + h - q/h^2) = 0, \\ -c\frac{\partial h}{\partial x} + \frac{\partial q}{\partial x} = 0. \end{aligned}\right\} \tag{2.3}$$

where the * has been omitted for convenience. One can consider the solitary wave solutions as homoclinic orbits in the phase space of $(h^*, h_x^*, h_{xx}^*, q^*)$ which connect the fixed point (1,0,0,1) to itself (Demekhin & Shkadov 1985). If one integrates the kinematic equation to yield

$$-c^* h^* + q^* = 1 - c^* \tag{2.4}$$

the averaged flow rate q^* can then be eliminated and the phase space is reduced to (h^*, h_x^*, h_{xx}^*). The linearized Jacobian about the fixed point (1,0,0) yields the spatial eigenvalues shown in table 1. It is clear that for all δ, a positive real eigenvalue $2m$ and a complex conjugate $-m \pm i\beta$ with a negative real part exist. The homoclinic orbit hence represents the special case when the one-dimensional unstable manifold

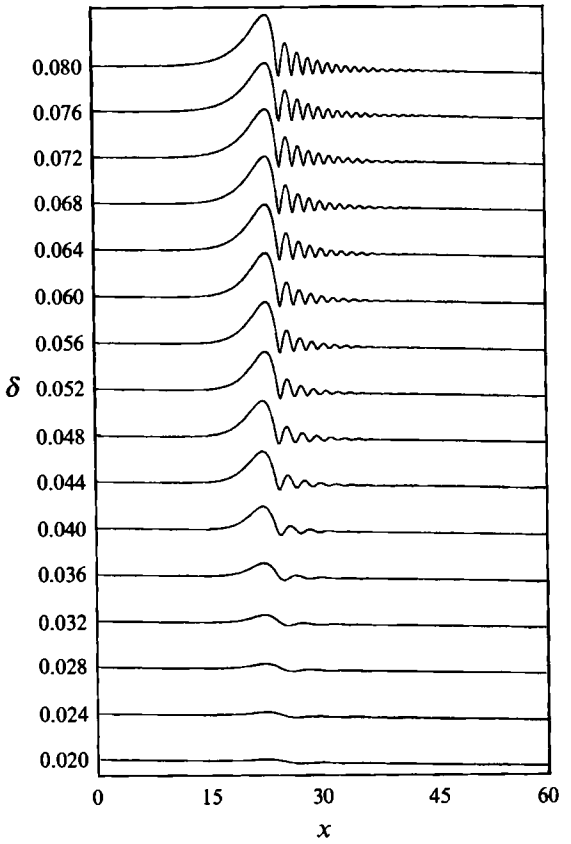

FIGURE 3. The solitary pulse family as a function of δ. All substrates are of unit thickness.

joins the two-dimensional stable manifold. This is a codimension-one bifurcation and the homoclinic orbit exists at a unique 'nonlinear eigenvalue' c^*, corresponding to the speed, for any give δ. There is hence a single solitary pulse for a given δ and δ parameterizes a family of such pulses as we learned from the KS equation. This is the family shown in figure 3. The speed and the pulse height h_m of the solitary wave are also included in table 1. As is consistent with our previous argument, we find the ratio $(c^* - 3)/(h_m - 1)$ to be constant at about 2.4 for $\delta < 0.05$, close to the 2.25 predicted from the KS solitary pulse. Even at higher δ, this ratio only decreases to about 2.0 for the largest solitary pulse at $\delta = 0.09$. This is quite remarkable since, as shown in table 1, the pulse amplitude at $\delta = 0.09$ is 3.36 times the substrate thickness and the weakly nonlinear KS scaling is definitely incorrect in this region. Another curious result is that the speed c^* and amplitude h_m of the solitary pulse measured from the wall seem to approach constant asymptotes at large δ. The width w of this pulse and the area A within the hump, after substracting the flat substrate film, still vary significantly at large δ, as is evident in figure 3. The small-δ solitary pulses correspond to the KS limit and their amplitude-shrinking and length-stretching KS scaling are quite evident in figure 3.

We note that the speeds of the solitary pulses are much larger than the linear phase speed and the finite-amplitude sinusoidal waves, both of which travel slower than three times the average velocity, the unit for wave speed in the averaged equation

δ	w	A	c^*	h_m	m	β	γ	R	S	θ (rad)	l^*	l_2	c_2^*	$\hat{h}_c(0)$ (theory)	$\hat{h}_c(0)$ (measured)
0.03	15.6	1.38	3.65	1.27	0.277	1.044	0.021	2.37	2.12	1.11	9.4	8.61	3.57	0.14	0.26
0.04	15.9	4.39	5.19	1.93	0.311	1.853	0.018	44.09	17.6	2.29	8.0	6.54	4.68	0.13	0.52
0.05	21.4	9.35	6.87	2.68	0.236	2.855	0.047	80.86	41.3	2.66	7.2	5.59	6.34	0.35	0.89
0.06	26.7	12.7	7.36	2.98	0.190	3.380	0.056	58.17	49.0	−1.07	5.3	5.37	7.00	0.46	0.94
0.07	31.2	15.4	7.56	3.17	0.161	3.762	0.058	37.54	50.9	2.18	4.9	5.25	7.30	0.49	0.94
0.08	34.5	17.8	7.65	3.28	0.140	4.077	0.057	24.38	48.8	0.57	4.9	5.15	7.51	0.48	
0.09	36.9	20.1	7.69	3.36	0.124	4.348	0.056	16.30	44.0	−1.46	5.1	5.09	7.65	0.46	
∞			7.71	3.42			0.056				5.0			0.46	

TABLE 1. Coefficients for the single-hump and double-hump solitary pulse families with $\chi = 1$

(Demekhin & Shkadov 1985 and Chang *et al.* 1993*a*). The fact that the positive eigenvalue is real and the complex conjugate has a negative real part also dictates the shape of the solitary wave. As is evident from figure 3, while the back slope is smooth and monotonic in the negative-x direction, a rapid drop in the positive x-direction is followed by diminishing oscillations. These oscillations, sometimes known as bow waves, are unique to solitary pulses on thin films. For near-critical conditions, Chang (1986) has associated them to the neutral waves of a flat film which are dominated by capillarity. They are hence known sometimes as capillary ripples. We shall show that these ripples have a profound effect on the interaction dynamics between pulses. If we choose the absolute maximum of the pulse h_m to lie at the origin, the two tails of the pulse, the monotonic back tail and the oscillatory front tail, can be approximated by

$$\left.\begin{aligned} h_f(x) - 1 &= A\cos(\beta x + \phi_0)\mathrm{e}^{-mx} \quad \text{as} \quad x \to \infty, \\ h_b(x) - 1 &= B\mathrm{e}^{2mx} \quad \text{as} \quad x \to -\infty. \end{aligned}\right\} \tag{2.5}$$

The parameters A, B and ϕ_0 are functions only of δ and they can be easily obtained from the constructed solitary pulses. These expressions for the tail greatly simplify the computational effort of our theory.

The condition (2.4) implies that h and q of each solitary pulse member in the family have been normalized to unity at the flat-film limit of $x \to \pm\infty$. The parameter δ is actually defined by the Nusselt thickness h_N of this flat-film limit. However, as is evident from figure 1, the flat-film substrate in the vicinity of each solitary pulse is slightly different and each is much smaller than the original flat film near the inlet flow rate. This difference in the substrate is due to the fact that the solitary pulses are mass-carrying and the flat-film sections do not necessarily have the same flow rate and, hence, the same thickness. (This fact was first realized by Nakaya 1989.) We shall hence model each pulse in figure 1 as a stationary solitary pulse on a particular substrate and moving at a particular speed. Since $h(\pm\infty)$ and $q(\pm\infty)$ have been normalized to unity in (2.3) and (2.4), δ then represents a parameterization of the substrate thickness of a pulse for a given fluid. Equivalently, each pulse in figure 1 corresponds to a member of the family in figure 3. The dynamics we observed in figure 2 is then due to interaction among different pulse members of figure 3. These interactions are driven mostly by the occasional large pulse which results from a coalescence event. (Three are seen in figure 1 at $x = 410$, 480 and 780.) Since each large pulse travels much faster than its smaller neighbours, it quickly tears away from its back neighbour and encroaches on its front one. The dominant interaction is hence a binary one between a larger pulse and its smaller front neighbour. As the larger pulse approaches its front neighbour, it loses mass as the two pulses sit on different substrates and the drained liquid is used to coat the thinner substrate. If the initial separation between the two pulses is sufficiently large, the drainage will stop when the two substrates are of the same thickness and the two pulses are identical. These two identical pulses will still attract or repel each other and this interaction between two identical pulses will determine whether the next coalescence will take place. A critical coalescence criterion is hence the key to fully understanding the solitary pulse dynamics and one will be developed here.

Our theory focuses on the binary interaction between a large pulse and its smaller front neighbour at a given δ. With just two pulses, the substrate thickness, unlike that in figure 1, remains at unity away from the pulses. The front pulse is the true solitary pulse for the given δ value and is used as a reference pulse. In a coordinate system moving at the same speed as this reference pulse, it remains stationary. Since our

computations for the binary interaction will be carried out in this moving coordinate system, the front pulse will be called the stationary pulse. The larger pulse, on the other hand, is not the true solitary pulse solution at that δ. However, we shall assume that it is a solitary pulse for a higher δ and hence sits on a local segment of substrate whose thickness is greater than unity. This back pulse is hence known as the excited pulse and it has a larger substrate thickness, amplitude and speed than the stationary pulse. As a result, it advances and decays in the moving coordinates as all three quantitites decrease. During this decay stage, we assume that the excited pulse corresponds quasi-steadily to a member of the pulse family at each moment. The decay dynamics is then an evolution of the excited pulse through the family till the stationary member at the particular δ is reached. This quasi-steady decay will be verified by numerical experiments. After resolving the decay dynamics of the excited pulse towards the stationary pulse, the theory then describes the interaction of two identical stationary pulses on the same substrate of unit thickness. Near the inlet when the initial separation is small, the excited pulse may not decay completely to one that is identical to its front neighbour before coalescence takes place. We shall show, however, that the excited pulse decays very rapidly and our theory is valid for separations no shorter than two or three pulse widths. It is hence quite accurate from $x = 400$ in figure 1 and $x' = 40$ cm in figure 2.

For a given flow condition, viz. at a given δ value, when we numerically place the constructed solitary pulse on a unit substrate in the moving frame with speed c^*, it remains stationary provided other disturbances are not imposed. It should be noted, however, that the flat substrate region is strictly unstable and sinusoidal disturbances will nucleate with any slight perturbation. However, since the latter waves travel much slower than the solitary pulse, they are quickly swept into the pulse as shown in figure 4, where uncharacteristically large sinusoidal waves have been numerically placed in front of a pulse. During interaction with the sinusoidal 'phase waves', the change in the solitary pulse is almost imperceptible. Its speed is only slightly perturbed during and after absorbing the sinusoidal waves. We can hence omit the effect of the substrate sinusoidal waves on the solitary wave dynamics. This has also been observed by Liu & Gollub (1994) whose experiments show that the solitary waves tend to sweep the surface clean of any small fluctuations.

To study and demonstrate the binary interaction leading to coalescence, a larger solitary pulse is placed behind the original stationary one. As shown in figure 5*a*, when the separation between the pulses is smaller than a critical value, the two pulses will attract each other and coalesce irreversibly to form a single large pulse. If the initial separation is large, there will be some transient interaction but the two pulses will eventually repel each other and yield two independent pulses, as shown in figure 5*b*. These two pulses will be separated by a constant separation and are known as a 'bounded pair' as shown in figure 6*a*. After some careful numerical experiments, it is possible to obtain the critical initial separation delineating coalescence and repulsion for a given pair of excited and stationary pulses, and one sees that the two pulses form a far closer 'bounded pair' than the repulsion case which resembles the two-hump solitary pulse shown in figure 6. This particular bounded pair hence represents the transition state for coalescence. Identical stationary pulses coalesce if their separation is smaller than the critical distance l^* represented by the separation between the two humps of the transition-state bounded pair.

It is important to note that this critical distance l^* for the coalescence of two identical pulses on the same substrate is different from the critical initial separation observed in figure 5 between a given pair of excited pulses and its stationary front

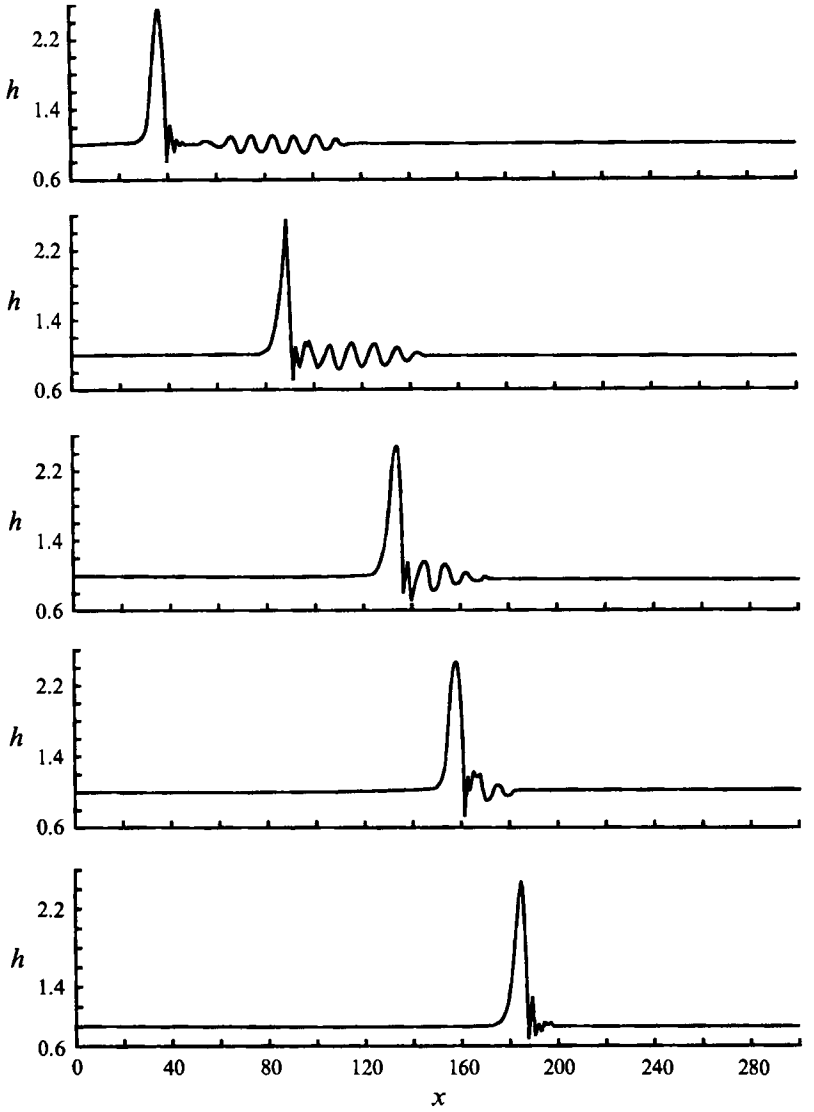

FIGURE 4. Interaction between a solitary pulse and sinusoidal phase waves. The frames are taken at equal intervals in a fixed laboratory frame. Note that the speed and shape of the pulse remains unaffected by the interaction.

neighbour. The latter critical separation is a function of the initial difference in the amplitudes of the two pulses and it approaches l^* as the difference approaches zero. The objective of our theory is to estimate how the critical distance depends on the amplitude difference. Using the front stationary pulse as the reference pulse, this difference can then be termed the 'degree of excitation' of the back pulse which can be measured by $\hat{h}, \hat{c}$ or $\hat{\chi}$, the difference in amplitude, speed or substrate thickness, respectively. Each measure is equivalent since the excited back pulse is a member of the one-parameter solitary pulse family at every instant in its decay. The dependence of the critical separation on the degree of excitation of the back pulse explains why some near encounters far from the inlet in the world lines of figure 2 do not lead

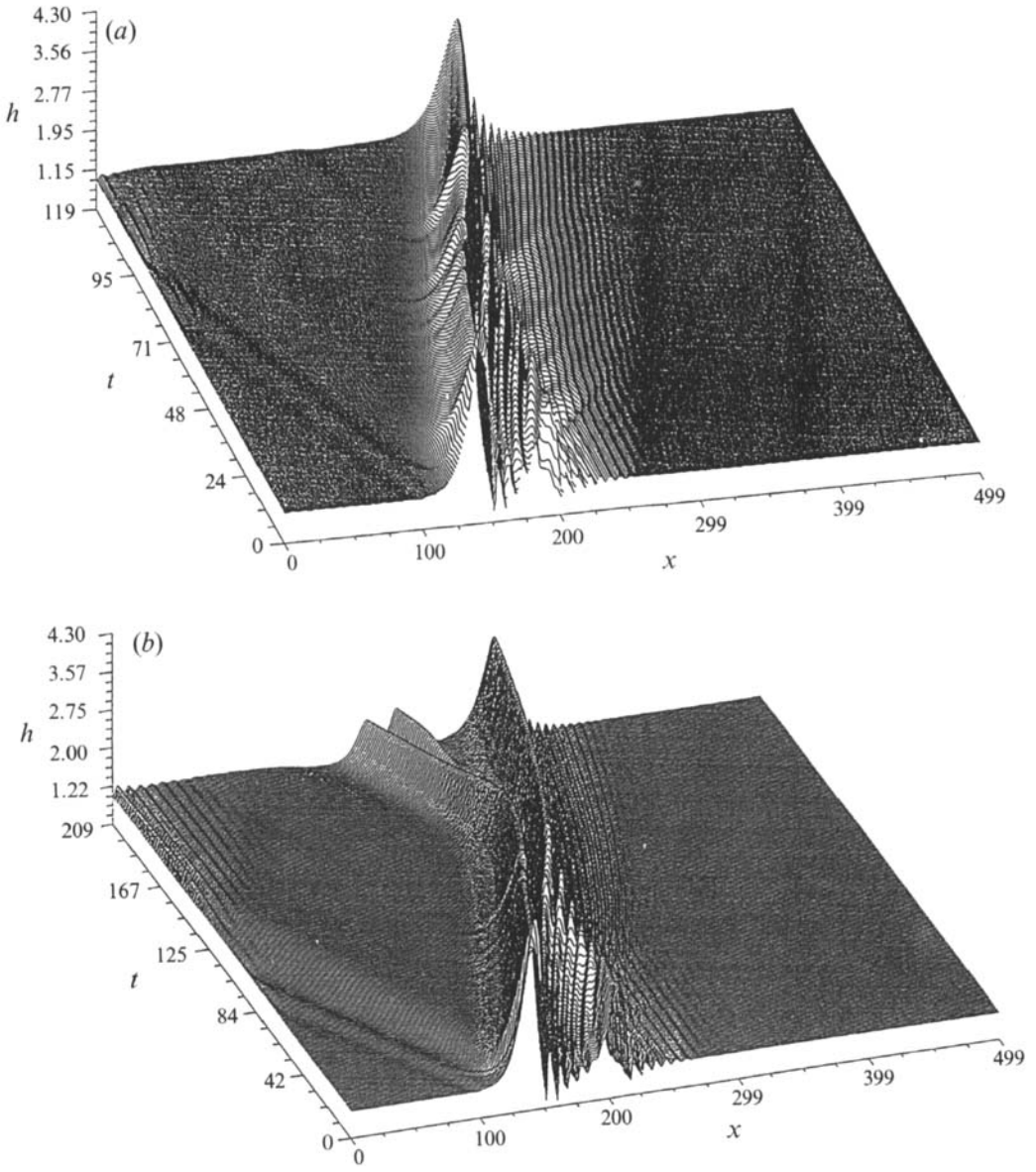

FIGURE 5. Two interaction experiments showing (*a*) coalescence and (*b*) repulsion for $\delta = 0.05$ in a frame moving with the speed of the front stationary pulse $c^*(\delta)$. In both cases, the initial amplitudes are the same with the back pulse excited but the inital separations are different.

to coalescence even though the two pulses come as close as those that do coalesce further upstream. Each prior coalescence gives rise to a pulse of roughly equal degree of excitation but a coalesced pulse far downstream is simply further from its front neighbour. The next coalescence may not occur even if the two pulses approach each other since the back pulse has drained most of its fluid, viz. the initial separation exceeds the critical value. A more detailed depiction of the coalescence event from our numerical experiments is shown in figure 7. It is seen that, at the initial large separation, the excited pulse 1 at the back is oblivious to the stationary pulse 2 in

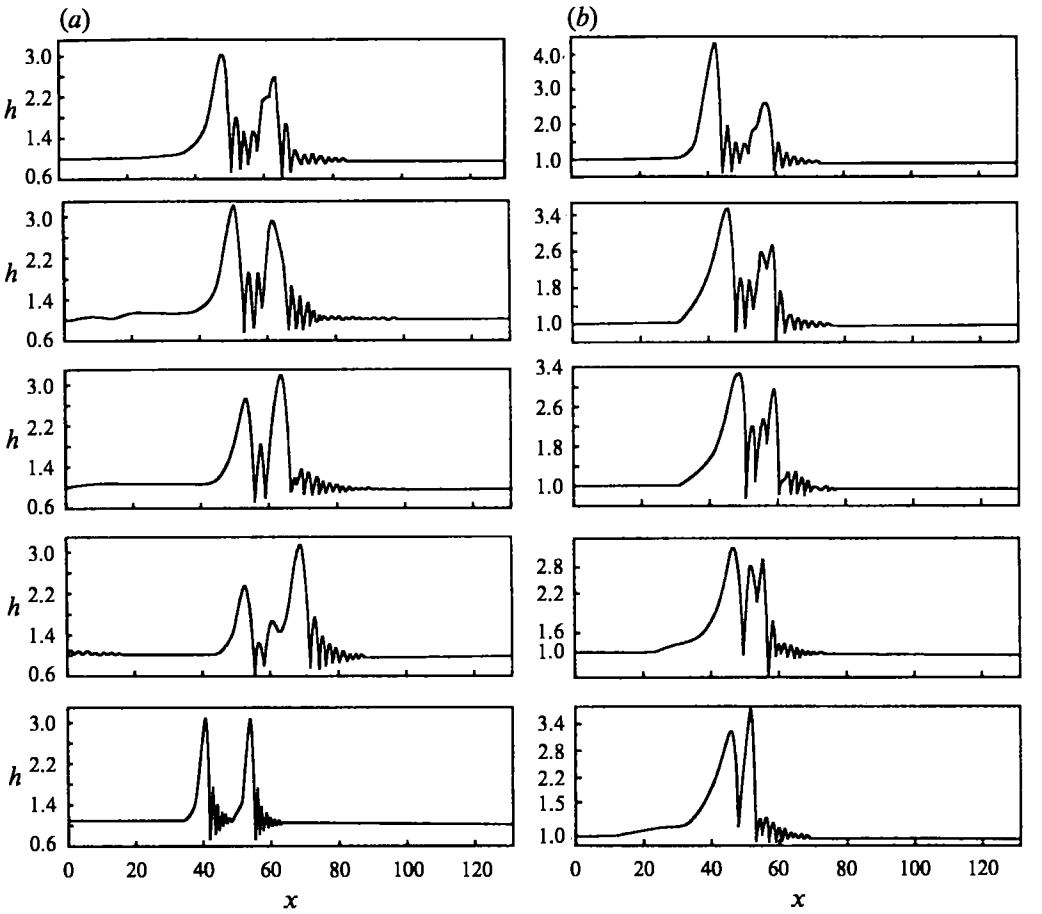

FIGURE 6. (*a*) The repulsion case of figure 5(*b*) resulting finally in a bounded pair with large separation and (*b*) the critical initial separation that results in a two-hump pulse.

front and its amplitude decays in a unique linear fashion, which will be scrutinized in a latter section, as it catches up with the stationary pulse. The stationary pulse 2 is also unaffected by the decay dynamics of the excited pulse during the transient period. When two pulses are sufficiently close, however, the short-range attractive interaction takes over and causes the two pulses to coalesce to form pulse 3.

The decay dynamics of the excited pulse at the back in figure 7 is extremely important. At any given instant, it resembles a solitary pulse of a larger δ in figure 3. The approach towards the stationary pulse of the actual δ in the experiment roughly corresponds to a quasi-steady evolution along the family of solitary pulses in figure 3 towards the one corresponding to the actual δ value. This is further corroborated in figure 8 where the decay dynamics is compared to the solitary pulse branch represented by $c^*(\delta)$ and $h_m(\delta)$. (Note the similarity in the shapes of the two curves $c^*(\delta)$ and $h_m(\delta)$. This is another manifestation of the fact that $(c^* - 3)/(h_m - 1)$ is approximately constant.) Ideally, the instantaneous δ should be determined from the measured instantaneous film thickness behind the pulse. However, we have found it easier to determine δ by measuring the area A under the pulse, which is a larger number than the thickness, and using table 1 to find the corresponding δ. It suffices to view δ as a measure of the decay time and c^* and h_m seem to track the c^* and

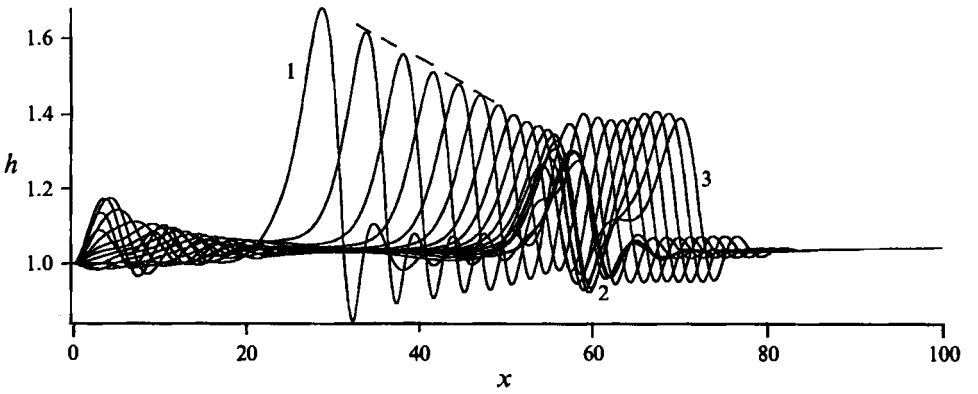

FIGURE 7. A different depicition of the interaction in figure 5(*a*) that leads to coalescence. Note the linear decay of the excited back pulse. Pulse 1 is the initial excited pulse and pulse 2 the initial stationary pulse. Pulse 3 is the coalesced pulse.

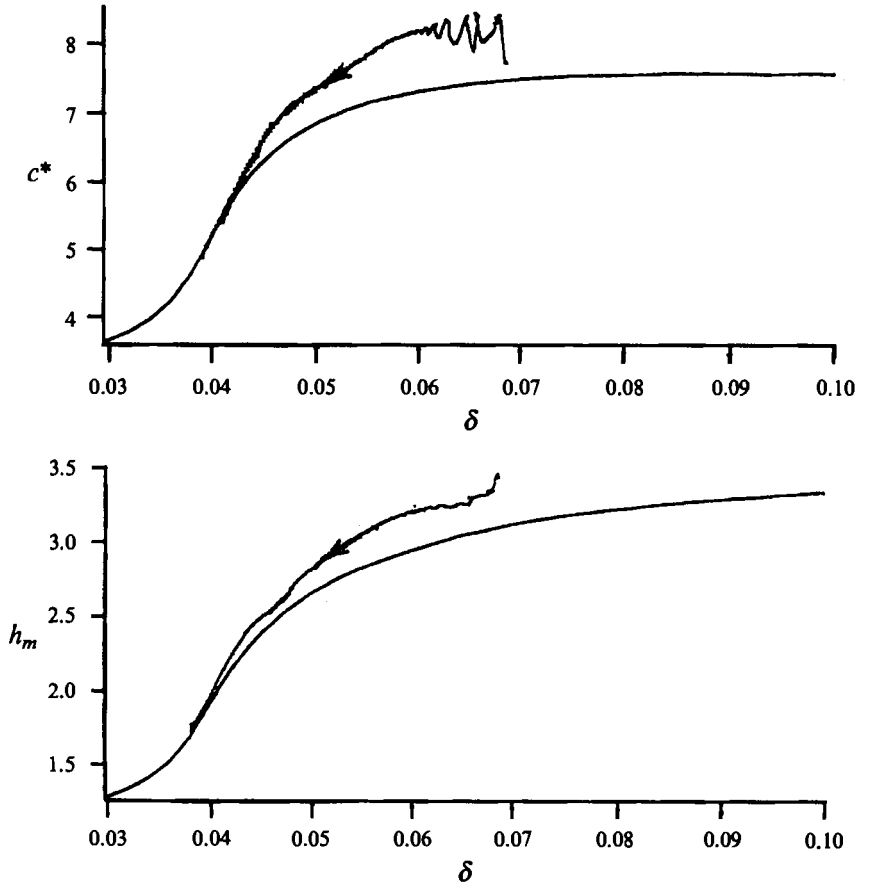

FIGURE 8. Decay of the excited pulse in figure 7 along the solitary pulse family of figure 3. The instantaneous δ values are computed from transformation (3.4) by measuring the area A under the pulse and using table 1.

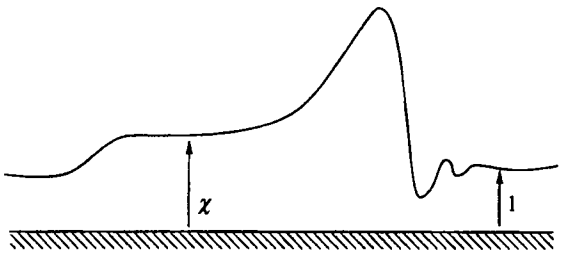

FIGURE 9. Schematic of an excited pulse with a back substrate thickness χ that is larger than the unit thickness in front.

h_m of the solitary pulse family in figure 3 very closely. The excited solitary pulse is observed to perch on a back substrate layer of thickness χ that is thicker than the unit value corresponding to the actual δ. (See the coalesced pulse 3 of figure 7 where the back substrate is at its thickest value.) An exaggerated caricature of this excited pulse is depicted in figure 9. As the excited pulse decays, the raised substrate thins towards unity while liquid drains out of the pulse as it approaches the true stationary one. A small shock is created behind due to this drainage and it propagates backward relative to the pulse. This small shock is also evident in figures 5, 6 and 7. Such a shock actually corresponds to an interaction of the solitary pulse with radiation modes spanned by its continuous spectrum. However, in this preliminary study, we shall approximate the drainage mechanism with a different formulation involving the point spectra.

A qualitative understanding of the evolution dynamics shown in figures 1 and 2 has now emerged. After each coalescence, an excited pulse which resembles a stationary pulse at a higher δ is created and travels faster than its smaller front neighbour. It will hence shorten the separation from its stationary front neighbour. However, given sufficient separation from its front neighbour, the excited pulse will decay quasi-steadily in amplitude and speed towards a true stationary pulse and the separation will eventually reach an asymptotic value when the two pulses travel at the same speed. If this asymptotic value is smaller than a critical separation, short-range attractive forces will cause the two pulses to coalesce. Otherwise, two independent stationary pulses will result. Since the initial separation between an excited pulse and its front neighbour will increase downstream on average as more and more pulses are annihilated by coalescence while the 'degree of excitation' due to the coalescence of two nearly stationary pulses remains the same, an equilibrium separation will eventually be reached such that additional coalescence is not possible. It is then clear that the most important key to the understanding of the pulse dynamics is the binary interaction between an excited pulse and a stationary pulse in front. We shall develop an analytical theory that describes the long-range decay of the excited pulse and the relatively short-range interaction of the two pulses. In particular, an estimate of the critical separation l^* will be constructed. This binary theory promises to elucidate the more complex dynamics in figures 1 and 2.

3. Spectrum of the solitary pulse

It was realized a few years ago (Kawahara & Toh 1988; Elphick *et al.* 1991; Chang *et al.* 1993*b*; Balmforth, Ierley & Spiegel 1994) that binary pulse interaction can be described by a coherent structure theory that describes the interaction between

two localized pulses due to the overlap between their tails. However, implicit in this theory is the assumption that the pulses must remain coherent, viz. stable to disturbances that decay to zero away from the pulses. If this stability is violated, the pulses will break up (split) and it is not meaningful to study their interaction. All the aforementioned attempts focused on the application of coherent structure theory to the solitary wave of the Kuramoto–Sivashinsky (KS) equation and its generalization. However, integration of the KS equation (Frisch, Zhen & Thual 1986; Kawahara & Toh 1988; Jayaprakash, Hayot & Pandit 1993, among many others) yields cellular structures but they do not resemble the solitary waves of the KS equation constructed by Chang *et al.* (1993*b*). This suggests that the solitary waves in figure 3 are not stable to localized disturbances at low δ, when the averaged equations reduce to the KS equation.

The eigenvalue problem that determines the stability of a solitary pulse to localized disturbances is

$$\left.\begin{aligned} \boldsymbol{L}\psi &= \lambda\psi, \\ \psi \text{ bounded as } x &\to \pm\infty, \end{aligned}\right\} \tag{3.1}$$

where the components of the vector function ψ denote the deviation flow rate $\hat{q}$ and the deviation height $\hat{h}$,

$$\psi = (\hat{q}, \hat{h}),$$

$$\boldsymbol{L} = \begin{pmatrix} \mathrm{L}_1 & \mathrm{L}_2 \\ -\dfrac{\mathrm{d}}{\mathrm{d}x} & c^* \dfrac{\mathrm{d}}{\mathrm{d}x} \end{pmatrix},$$

$$\mathrm{L}_1 = c^* \frac{\mathrm{d}}{\mathrm{d}x} - \frac{1}{5\delta h^{*2}} - \frac{6}{5}\frac{\mathrm{d}}{\mathrm{d}x}(2q^*/h^*),$$

$$\mathrm{L}_2 = \frac{1}{5\delta}\left[h^* \frac{\mathrm{d}^3}{\mathrm{d}x^3} + h^*_{xxx} + 1 + 2q^*/h^{*3}\right] + \frac{6}{5}\frac{\mathrm{d}}{\mathrm{d}x}[(q^*/h^*)^2],$$

where (h^*, q^*) denote the solitary pulse.

We note that part of the spectrum of $\boldsymbol{L}$ can be continuous. This continuous spectrum is unstable as its eigenfunctions approach the oscillatory primary waves of the flat-film substrate at the infinities. The unstable primary instability of the flat film of the averaged equations has been computed by Shkadov (1967). Although this continuous part of the spectrum is unstable, our numerical experiment in figure 4 indicates that the sinusoidal waves on the flat substrate that are triggered are quickly swept up by a solitary pulse which, in turn, is almost unaffected by these sinusoidal waves. We hence omit the continuous spectrum and focus instead on the point spectra of the solitary pulse defined by (3.1). Ideally, the drainage process in figure 7 should be studied with the continuous spectrum but this will await a later, more detailed, analysis. An eigenmode ψ_2 of this point spectrum of the solitary pulse dominates the drainage dynamics. Unlike other point eigenvalues, however, this eigenfunction is bounded but does not decay to zero at the infinities. It requires an ad hoc formulation, which is not rigorously correct, to permit an analysis of the decay dynamics from the step change in the substrate thickness shown in figure 9. The associated change in the average thickness seems to be only possible for interfacial dynamics which contains both the flow and kinematic dynamics, as in the averaged equations.

The spectrum defined by (3.1) contains two zero eigenvalues due to the symmetries of the solitary pulse. Perturbations to the solitary pulse that break these symmetries will shift these two eigenvalues but their real parts remain small. These perturbations are system perturbations and not the transient distubances in the classical linear stability theory. They correspond to the effect of a perturbation operator L' on a simple zero eigenvalue of L, viz. we would like to resolve the near-neutral spectrum of $L+L'$ given that L has some zero eigenvalues. In our case, the perturbation operator is in the form of another solitary pulse or a change in the substrate thickness in front of the pulse (a hydraulic jump). Provided that the other point eigenvalues are stable and bounded away from the imaginary axis in the complex plane, these two modes will dominate the dynamics of a pulse even after they are shifted by the imposed perturbations.

The first pertinent symmetry is the translational symmetry – if $(q^*,h^*)(x)$ is a solution, so should $(q^*,h^*)(x-x_0)$ be for any arbitrary shift x_0. Hence, for a known pulse solution, a one-parameter family of pulses parameterized by x_0 can be generated simply by shifting. Put another way, if one perturbs a stationary solitary pulse by translating it slightly, the degeneracy that arises from the continuous family of solutions implies that this motion is in the direction of an eigenfunction with a zero eigenvalue. More precisely, for x_0 small

$$\begin{pmatrix} q^* \\ h^* \end{pmatrix}(x-x_0) \sim \begin{pmatrix} q^* \\ h^* \end{pmatrix}(x) - x_0 \begin{pmatrix} q^*_x \\ h^*_x \end{pmatrix}(x) \tag{3.2}$$

and

$$\psi_1 = \begin{pmatrix} q^*_x \\ h^*_x \end{pmatrix}(x) \tag{3.3}$$

is a null eigenfunction of L. Since q^* and h^* approach unity at the infinities, the vanishing-derivative boundary conditions are obviously satisfied. One component h^*_x of ψ_1 is shown in figure 10 for a particular pulse.

The second symmetry that generates 'zero dynamics' is more subtle. It corresponds to the degeneracy related to the family of solitary pulses in figure 3. As mentioned earlier, each member of the family is normalized such that $h^*(\pm\infty)$ and $q^*(\pm\infty)$ are unity. The substrate thickness and its corresponding flow rate are then represented by δ. In turn, one can fix δ and allow $h^*(\pm\infty)$ and $q^*(\pm\infty)$ to vary. The asymptotic film height and flow rate cannot vary independently due to mass conservation in (2.3) and (2.4) and it is convenient to denote $h^*(\pm\infty)$ as χ. The value of δ can be arbitrarily fixed but is usually given the flat-film value at the inlet, viz. based on the inlet flow rate. Physically, however, the δ-parameterized family and the χ-parameterized family are identical and there must be a transformation that maps one family to the other. For a given flow condition, one simply cannot vary χ and δ independently. This also implies that in our numerical experiment in figure 1 which integrates (2.1) at a fixed δ value, there is actually a one-parameter family of solitary pulses parameterized by the substrate thickness χ and the spectrum of each solitary pulse member of the family must contain a zero eigenvalue due to this degeneracy that arises because the local substrate thickness and flow rate are not specified in the defining equations (2.3) for the solitary pulse. The transformation that transforms the δ-parameterized family of figure 3 to a χ-parameterized family at fixed δ can be determined from a simple

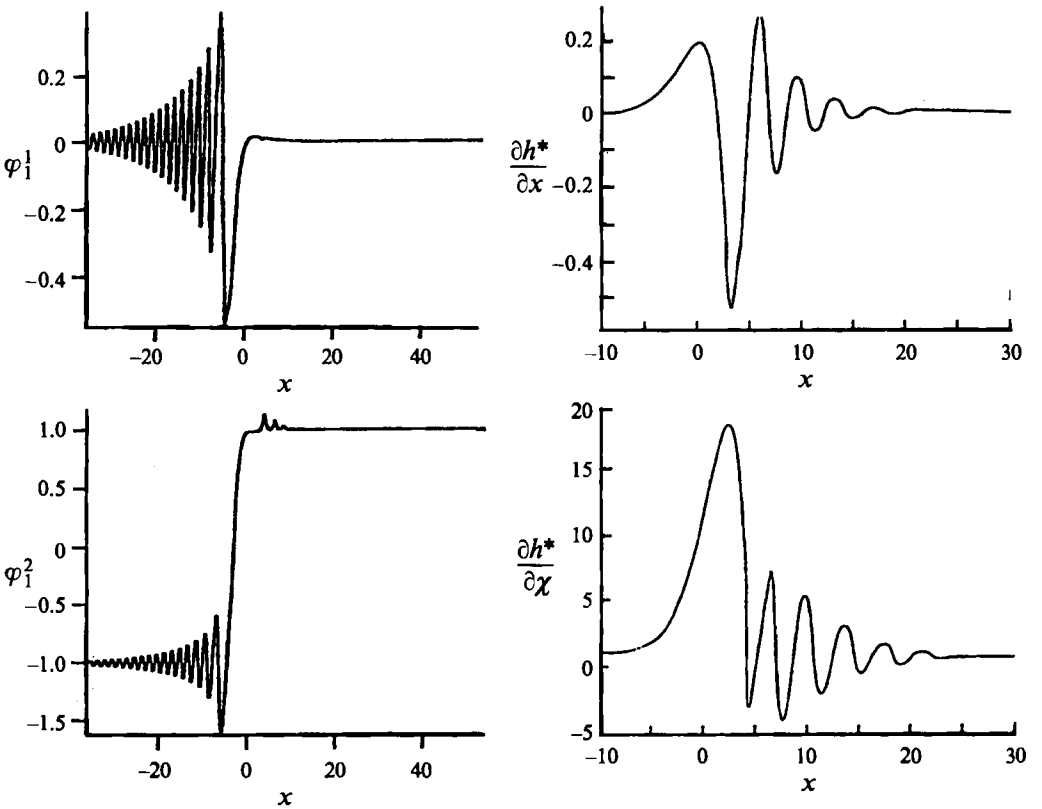

FIGURE 10. The two components of the adjoint eigenfunction φ_1 and the $\hat{h}$ components of ψ_1 and ψ_2 at $\delta = 0.07$.

application of the π-theorem,

$$\left.\begin{aligned} h^*(x;\delta,\chi) &= \chi h^*(x\chi^{-1/3};\delta\chi^{11/3},1),\\ q^*(x;\delta,\chi) &= \chi^3 q^*(x\chi^{-1/3};\delta\chi^{11/3},1),\\ c^*(\delta,\chi) &= \chi^2 c^*(\delta\chi^{11/3},1), \end{aligned}\right\} \tag{3.4}$$

and the defining equations (2.3) for the solitary pulse with $h^*(\pm\infty) = \chi$ are invariant under this transformation. Note that the solitary speed c^* must also be transformed and the spatial coordinate x stretched. This transformation allows us to transform the δ-parameterized family of figure 3 where $\chi = 1$ to a family parameterized by χ for any given δ. Since the simulation in figure 1 is carried out for a fixed δ, each stationary solitary pulse observed there is then a member of the latter family. There is, of course, an infinite number of such solitary pulses possible with different substrate thicknesses. The variation in the substrate thickness from one pulse to another is quite apparent in figure 1. We note that in the binary interaction experiment of figures 5, 6 and 7, the final substrate thickness, regardless of whether coalescence takes place, is unity since there are only one or two solitary pulses on the film. This is, of course, not true in figure 1 where numerous pulses exist.

For a given δ, the translational invariance that generates a one-parameter family yields a zero eigenvalue. The invariance to transformation (3.4) also yields a one-

parameter family and hence a zero eigenvalue of $\mathscr{L}$ related to this symmetry is expected. The corresponding eigenfunctions are

$$\psi_2 = \begin{pmatrix} q_\chi^* \\ h_\chi^* \end{pmatrix}(x,\chi) \tag{3.5}$$

one component of which is shown in figure 10. It measures the changes in q and h as one moves through the pulse family of figure 3. Since the decay of an excited pulse corresponds to such a quasi-steady motion through the family, this mode determines the decay rate. In fact, h_χ^* specifies how much fluid drains out of the excited pulse of figure 9 as it decays. In the present theory, we shall set χ to unity in the derivative in (3.5). By taking the derivative of (2.3) with respect to c^* and by using (2.4) one immediately sees that

$$\boldsymbol{L}\begin{pmatrix} q_c^* \\ h_c^* \end{pmatrix} = \psi_1$$

where subscript c denotes derivative with respect to c^*. It is more convenient to use ψ_2 and since

$$\psi_2 = \frac{\partial c^*}{\partial \chi}(\chi,\delta)\begin{pmatrix} q_c^* \\ h_c^* \end{pmatrix},$$

it immediately follows that ψ_2 is a generalized null eigenfunction such that for a given χ (or δ),

$$\boldsymbol{L}\psi_2 = \alpha\psi_1, \tag{3.6}$$

where the parameter α is

$$\alpha = \frac{\partial c^*}{\partial \chi}(\chi,\delta)$$

and it corresponds to a derivative along the solitary pulse family. Note also that ψ_2 has vanishing derivatives at the infinities but decays to the unit constant itself. This is because there is a change in substrate thickness as one goes from one member of the family to another within the solitary pulse family parameterized by χ.

A detailed discussion of why the ψ_2 mode of the KS equation should be a generalized eigenfunction has been offered Elphick *et al.* (1991). We explore a more physical explanation here. The zero mode ψ_1 corresponds to a position mode related to the translational symmetry. Whenever the translational symmetry is broken by a perturbation, this mode is excited and the pulse is shifted. However, there is no correction to the speed of the pulse – it is not accelerated. The generalized zero mode ψ_2, on the other hand, corresponds to a speed mode since each member of the family in figure 3 has a different speed, c is a function of δ or χ. Since the dynamics of a position mode cannot be independent of the speed mode, these two zero modes cannot be independent and one must hence be a generalized zero mode.

The fact that ψ_2 approaches unity at the infinities presents a special problem. This implies that the disturbance that we would like to expand with ψ_1 and ψ_2 can also approach constant values at the infinities. Such non-integrable disturbances are not physical and do not correspond to any definable functional space. Equivalently, we cannot find a generalized adjoint eigenfunction to allow projection onto the generalized zero mode. A more proper analysis involves the continuous spectrum but we shall overcome this problem here by simply neglecting the tail ends of ψ_2 away from the pulse. This corresponds to localized disturbances and the implicit

assumption that the decay dynamics of figure 7 involves mass drainage from the pulse only and not the substrate thickness. The change in the pulse area is still well approximated by ψ_2 within the pulse width.

There are no other zero modes in the spectrum of the solitary pulse and we expect ψ_1 and ψ_2 to dominate the dynamic reaction of the pulse to perturbations. This is consistent with our observations from the numerical experiments. The slow decay dynamics of an excited wave corresponds to an excitation of the ψ_2 speed mode due to a change in the front substrate thickness as shown in figure 7. Although the translational invariance is also broken, the relative short range of the ψ_1 interaction implies that the position mode is not excited directly, as we shall demonstrate. The excited ψ_2 mode causes a transformation from a solitary pulse on substrate thickness χ to one on a unit substrate thickness in figure 7. In figure 1, this decay dynamics would connect solitary pulses on a thicker substrate χ_2 at the back to a thinner one χ_1 in the front. It is always a decay dynamics since the back substrate is always thicker than the front one after a coalescence event. The excited speed ψ_2 mode also shifts the position mode through the dependence between ψ_1 and ψ_2. This moves the back pulse closer to the front one until interaction between the two pulses through the position ψ_1 mode dominates over the ψ_2 decay dynamics – pulse–pulse interaction occurs on the same substrate thickness, unity in figures 5 to 7. This final interaction determines whether the two pulses will coalesce.

Although there are no other zero modes, the spectrum of L still contains non-zero point eigenvalues that are unrelated to any symmetry. These eigenvalues must all be stable and, in fact, bounded from the imaginary axis such that the perturbed zero modes are always dominant. Otherwise, the solitary pulses will lose their coherence and break up. Unlike the two zero modes, which cause a pulse to shift or accelerate without signifcantly changing its shape, the others are strongly shape altering and if they are excitable, it is not meaningful to apply our approach which presumes dynamics with small departures from the solitary pulse dominated by the two zero modes. We have carried out a detailed numerial analysis of the spectrum of L using a shooting method. The leading non-zero point eigenvalues of the solitary pulse are shown in figure 11. It is clear that for $\delta < 0.03$, this point eigenvalue is stable but of the same magnitude as the perturbed zero eigenvalues. It would hence dominate the pulse dynamics as much as the other two. While it is possible to include this mode so that there are three dominant modes, we shall develop a simpler theory here with just the two dominant modes generated by the system symmetries. We hence require δ to be larger than 0.03 which encompasses most realistic conditions but excludes the use of low-δ evolution equations.

To project the pulse dynamics on to the two zero modes, we require the null adjoint eigenfunctions. The definition of the adjoint operator is detailed in Appendix A. We shall simply denote it as $\boldsymbol{L}^\dagger$ here and, as Elphick *et al.* (1991) have discovered for the KS equation, we find two null adjoint eigenfunctions (see Appendix A)

$$\boldsymbol{L}^\dagger \boldsymbol{\varphi}_1 = 0, \quad \boldsymbol{L}^\dagger \boldsymbol{\varphi}_2 = 0, \tag{3.7}$$

where the two components of $\boldsymbol{\varphi}_1$ are shown in figure 10 while $\boldsymbol{\varphi}_2 = (0, d)^t$ where d is a constant. It is clear that, using the inner product of Appendix A over the infinite domain, $(\boldsymbol{\psi}_2, \boldsymbol{\varphi}_2) = \int_{-\infty}^{\infty} \boldsymbol{\psi}_2 \cdot \boldsymbol{\varphi}_2 \mathrm{d}x$ is unbounded and hence unacceptable. This again relates to the fact that $\boldsymbol{\psi}_2$, as shown in figure 10, is not square-integrable. However, if we define the inner product $(\cdot, \cdot)$ involving $\boldsymbol{\psi}_2$ to be only over the pulse width, we

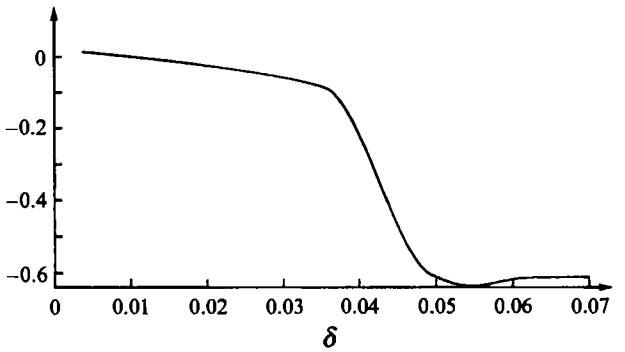

FIGURE 11. The leading non-zero point eigenvalue of the solitary pulse family in figure 3.

can always select a d such that

$$\left.\begin{aligned}(\psi_1, \varphi_1) = (\psi_2, \varphi_2) = 1,\\ (\psi_1, \varphi_2) = 0,\end{aligned}\right\} \tag{3.8}$$

where inner product involving ψ_1 is still over the infinite domain. We note that the biorthogonality condition in (3.8) does not include $(\psi_2, \varphi_1) = 0$. Even by restricting the domain of integration over the pulse width, this integral involving ψ_2 does not vanish. It is, however, a small number which we shall neglect. This anomaly arises because the operator L of (3.1) has a generalized zero mode while its 'adjoint' (3.7) does not. This peculiarity, in turn, originates from the non-square-integrable nature of ψ_2, the substrate/speed mode which controls fluid drainage from the pulse. A negligible (ψ_2, φ_1) corresponds to a decoupling between the drainage dynamics at large separation and the pulse–pulse interaction dynamics, which is controlled by ψ_1, at short separation. This is also consistent with the shrinking of the domain of integration in inner products involving ψ_2 – the drainage is unaffected by other pulses as is evident in the numerical simulation of figure 7.

We note that the second height component of the null adjoint eigenfunction φ_1 approaches constant values of opposite sign in opposite directions as seen in figure 10. This is consistent with the null adjoint eigenfunction constructed by Elphick *et al.* (1991) for the KS equation. The constant d for φ_2 such that $(\psi_2, \varphi_2) = 1$ can be easily estimated from symmetry (3.4). Let $x \in (a, b)$ be the pulse domain where the inner product is evaluated. This normalization then becomes

$$d\int_a^b \frac{\partial h}{\partial \chi}\mathrm{d}x = d\frac{\partial}{\partial \chi}\int_a^b h\mathrm{d}x = 1.$$

The integral $\int_a^b h\mathrm{d}x$ is simply the area under the pulse. However, from (3.4),

$$\begin{aligned}\int_a^b h(x;\delta,\chi)\mathrm{d}x &= \chi\int_a^b h(x\chi^{-1/3};\delta\chi^{11/3},1)\mathrm{d}x\\ &= \chi^{4/3}\int_{a'}^{b'} h(\xi;\delta\chi^{11/3},1)\mathrm{d}\xi = \chi^{4/3}A(\delta\chi^{11/3})\end{aligned}$$

where $\xi = x\chi^{-1/3}$ and $(b', a') = (b, a)\chi^{-1/3}$. We have neglected the area within the film beneath the pulse which is negligible compared to the pulse area. The quantity $A(\delta\chi^{11/3})$ is simply the area A in table 1 for the pulse family with $\chi = 1$. Hence,

at $\chi = 1$

$$\frac{\partial}{\partial \chi}\int_a^b h\mathrm{d}x = \tfrac{4}{3}A(\delta) + \tfrac{11}{3}\delta\frac{\mathrm{d}A}{\mathrm{d}\delta}$$

where $A(\delta)$ and $\mathrm{d}A/\mathrm{d}\delta$ can be obtained from table 1. The constant d is then

$$d = \left[\tfrac{4}{3}A(\delta) + \tfrac{11}{3}\delta\frac{\mathrm{d}A}{\mathrm{d}\delta}(\delta)\right]^{-1}.$$

We can now expand any solution to the averaged equations about the solitary pulse of an arbitrary χ (or δ) in the frame moving at the same speed as the reference pulse,

$$\begin{pmatrix}\hat{q}\\ \hat{h}\end{pmatrix}(x,t) = \begin{pmatrix}q\\ h\end{pmatrix}(x,t) - \begin{pmatrix}q^*\\ h^*\end{pmatrix}(x) \sim -x_0(t)\psi_1(x) + \hat{\chi}(t)\psi_2(x) \tag{3.9}$$

where $\hat{\chi}$ denotes deviation from the substrate thickness of the reference pulse and the amplitudes of the two zero modes have been represented by physically meaningful variables. The amplitude of the speed mode $\hat{\chi}(t)$ can also be transformed to $\hat{c}(t)$ from (3.4) where both $\hat{\chi}$ and $\hat{c}$ denote deviations from χ and c^* of the reference pulse. If we transform the averaged equation to a coordinate moving with the speed c^* of the reference solitary pulse in (3.9), substitute (3.9) into the resulting equation, linearize and take inner product with the null adjoint eigenfunctions, we obtain

$$\frac{\mathrm{d}}{\mathrm{d}t}\begin{pmatrix}x_0\\ \hat{\chi}\end{pmatrix} = \begin{pmatrix}0 & \alpha\\ 0 & 0\end{pmatrix}\begin{pmatrix}x_0\\ \hat{\chi}\end{pmatrix} \tag{3.10}$$

in the absence of any perturbation. The dependence between the position and speed modes has yielded the double-zero Jacobian of the projected linear dynamics. Without any perturbation, the solitary pulse remains stationary and x_0 and $\hat{\chi}$ are zero exactly. The pertinent dynamics observed in the previous section is then triggered when perturbations are imposed.

4. Inelastic coherent structure theory

We focus first on the decay dynamics corresponding to ψ_2. For a given δ, the solitary pulse on a unit substrate is taken to be the reference solitary pulse. The change in substrate thickness $(\chi - 1)$ behind the excited pulse, shown in figure 9 and seen as a backward propagating shock in figures 5 and 7, then represents a small and negligible step change in the substrate film but a significant mass sink. As the shock propagates backwards relative to the excited pulse, it coats the thinner substrate. The liquid mass required for this coating comes from the excited pulse. The coating rate is not constant since the capillary, inertial and viscous forces conspire in a quasi-steady manner such that the substrate thickness immediately behind the excited pulse decreases steadily. This explains why the back shock seen in figure 7 increases in amplitude away from the pulse: it is a reflection of the ever-decreasing substrate thickness as liquid mass is drained from the pulse. The rate of this mass loss can be easily determined. From the averaged equations (1), it is clear that the flow rate in the laboratory frame for a flat film of thickness χ is $q = \chi^3$. In a frame moving with the reference solitary speed, the flow rate becomes $q = \chi^3 - c^*\chi$. Consequently, the change in flow rate when a substrate exhibits a hydraulic jump from thickness χ to thickness unity is $\Delta q = \chi^3 - c^*\chi - (1 - c^*) \sim (3 - c^*)\hat{\chi}$ where $\hat{\chi} = \chi - 1 \ll 1$ is the 'degree of excitation' of the back pulse measured by the deviation substrate thickness. Since c^* is larger than 3, a net drainage from the pulse occurs. This sink can be

written as $(3-c)\hat{\chi}\delta(x^*)$ where x^* is the location of the jump in figure 9 and $\delta(x)$ is a Dirac delta function. The exact location of x^* is not important as long as it is not within the pulse. This perturbation to a single solitary pulse can then be described by the following perturbed and linearized version of the averaged equation in the moving frame,

$$\frac{\mathrm{d}}{\mathrm{d}t}\begin{pmatrix}\hat{q}\\ \hat{h}\end{pmatrix} = L\begin{pmatrix}\hat{q}\\ \hat{h}\end{pmatrix} + \begin{pmatrix}0\\ (3-c^*)\hat{\chi}\delta(x^*)\end{pmatrix}. \tag{4.1}$$

All other terms that arise due to the hydraulic jump are negligible compared to this point sink. Expanding $(\hat{q},\hat{h})$ by ψ_1 and ψ_2 as in (3.9), substituting into (4.1) and taking inner product $(\cdot,\cdot)$ with φ_1 and φ_2, one obtains the perturbed version of (3.10),

$$\frac{\mathrm{d}}{\mathrm{d}t}\begin{pmatrix}x_0\\ \hat{\chi}\end{pmatrix} = \begin{pmatrix}0 & \alpha\\ 0 & 0\end{pmatrix}\begin{pmatrix}x_0\\ \hat{\chi}\end{pmatrix} - \begin{pmatrix}0 & 0\\ 0 & \gamma\end{pmatrix}\begin{pmatrix}x_0\\ \hat{\chi}\end{pmatrix} \tag{4.2}$$

where $\gamma = \varphi_2^2(x^*)(c^*-3) = d(c^*-3)$ where d is the second $\hat{h}$ component of φ_2 and

$$\gamma = \frac{3(c^*-3)}{4A + 11\delta(\mathrm{d}A/\mathrm{d}\delta)}. \tag{4.3}$$

The values of the decay factor γ are tabulated in table 1. It also approaches a constant value for δ larger than 0.05.

In deriving (4.2), we have neglected the nonlinear terms in favour of the linear substrate perturbation term due to the hydraulic jump. In essence, we are ignoring the nonlinear interaction between the solitary pulse and the hydraulic jump. This is obviously valid when the jump is small such that $\gamma\hat{\chi}$ is larger than $O(|\hat{\chi}|^2)$ and $O(x_0|\hat{\chi}|)$ terms. This is generally true for the degrees of excitation involved but the omitted nonlinear terms are responsible for the larger errors and fluctuations seen in figure 8 when the degree of excitation is relatively large. We have also neglected the small jump in front of the excited pulse. It is more precise to model the decay of the excited pulse as the interaction of two shocks, with the front one corresponding to a shock travelling wave (a heteroclinic orbit) like the one constructed by Pumir *et al.* (1983). Such an endeavour requires far more effort, however, and we have approximated the front shock by a solitary wave (a homoclinic orbit). This is consistent with the small-$\hat{\chi}$ approximation.

One of the zero eigenvalues of the solitary pulse has hence been shifted by the presence of the jump in the substrate thickness which breaks the corresponding symmetry. This jump then drains fluid from the pulse which causes the pulse to evolve quasi-steadily into another solitary pulse with a thinner substrate. This is the observed slow decay dynamics of the excited pulse. The translation symmetry is also broken but the shift in the position zero mode is negligible for a small jump. Nevertheless, the slow decay induced by the shifted speed zero mode will trigger a shift in the position due to their linear dependence. The magnitude of γ is small as seen from table 1. The drainage ceases when the jump vanishes at $\hat{\chi} = 0$ but the drainage rate is related to how the area under the pulse changes as it moves through the family in figure 3. This change in area is captured by φ_2^2. The above slow decay requires that δ be in excess of 0.04 such that the omitted mode in figure 11 is larger in magnitude than γ. To justify the omitted nonlinear terms, we should also require the excitation $\hat{\chi}$ to be smaller than γ, which is easily satisfied for δ in excess of 0.04.

If these stipulations hold, (4.2) indicates that the slow decaying dynamics is linear such that the thinning of the raised substrate χ in figure 9 is governed by $\hat{\chi} \sim \exp(-\gamma t)$ where $\hat{\chi} = \chi - 1$. Since c^* and h_m can be expressed as a funciton of χ only during the

quasi-steady decay, we have

$$\hat{c} = c^*(\chi) - c^*(1) \sim \frac{\mathrm{d}c^*}{\mathrm{d}\chi}(1)\hat{\chi} = \alpha\hat{\chi},$$

$$\hat{h} = h_m(\chi) - h_m(1) \sim \frac{\mathrm{d}h_m}{\mathrm{d}\chi}(1)\hat{\chi}$$

and

$$\hat{c} = \frac{\mathrm{d}c^*}{\mathrm{d}h_m}(1)\hat{h}.$$

As mentioned in the previous section, we find from the constructed solitary pulse family that $c^* - 3 \sim 2.4(h_m - 1)$ and hence the derivative $\mathrm{d}c^*/\mathrm{d}h_m$ is approximately 2.4. To demonstrate this relationship more explicitly and to further verify that the decay dynamics evolves through the family of solitary pulses parameterized by δ, we show in figure 12 the evolution in amplitude and speed of the excited back pulse and the new pulse created by coalescence. The speeds and amplitudes of both decay exponentially in time but when cross-plotted, they lie on the same straight line close to the estimated correlation.

We note here that, since the derivatives of c^* and h_m with respect to δ or χ are non-zero, the second equation in (4.2) also implies that the speed, substrate thickness and amplitude all decay exponentially in time by the same rate:

$$\hat{c}, \hat{\chi}, \hat{h} \sim \exp(-\gamma t).$$

In figure 13, this unique decay dynamics is again verified by extracting the dynamics of the excited pulse in figure 7 for $\delta = 0.05$. The decay exponent of $\gamma = 0.047$ provides a very accurate description of the decay of both $\hat{c}$ and $\hat{h}$.

Another prediction of this theory for the decay of an excited pulse is that $\hat{h}$ decays linearly in space. Integrating the position x_0 equation in (4.2) that is coupled to the $\hat{\chi}$ speed mode, one obtains

$$x_0 \sim \frac{\hat{c}(0)}{\gamma}(1 - \mathrm{e}^{-\gamma t}) = x_\infty(1 - \mathrm{e}^{-\gamma t}) \tag{4.4}$$

which is also in agreement with the experimentally measured position of the excited pulse as it decays, as seen in figure 13. Since γ is small, the excited pulse is shifted significantly by an amount x_∞ from its original position in the moving frame. Combining the above equations, one obtains the linear amplitude decay in space:

$$\hat{h} \sim \hat{h}(0) - \gamma x_0 \hat{h}_0/\hat{c}(0) = \hat{h}(0)(1 - x_0/x_\infty). \tag{4.5}$$

In figure 7, the initial excitation, as measured by $\hat{c}(0)$, is approximately 3.0 which yields a predicted shift of $x_\infty = 60$. This is in agreement with the measured x_∞ in figure 13. This predicted x_∞ also suggests that the excited amplitude decays linearly in space at $\delta = 0.05$ by a slope of 0.017 which is in good agreement with the simulations shown in figures 7 and 13, even when the excited pulse has come very close to the stationary pulse in front of it. The measured linear decay in figure 7 has a slope of approximately 0.02. This estimated value of x_∞ is about three times the pulse width w at $\delta = 0.05$. This implies that any excited pulse which is roughly twice the amplitude of the stationary pulse in front will have sufficient space to decay towards a stationary one if the initial separation is more than three times the pulse width. This is true for all δ values and hence, as long as the initial separation is more than three times the pulse width, the final interaction is between two identical pulses on

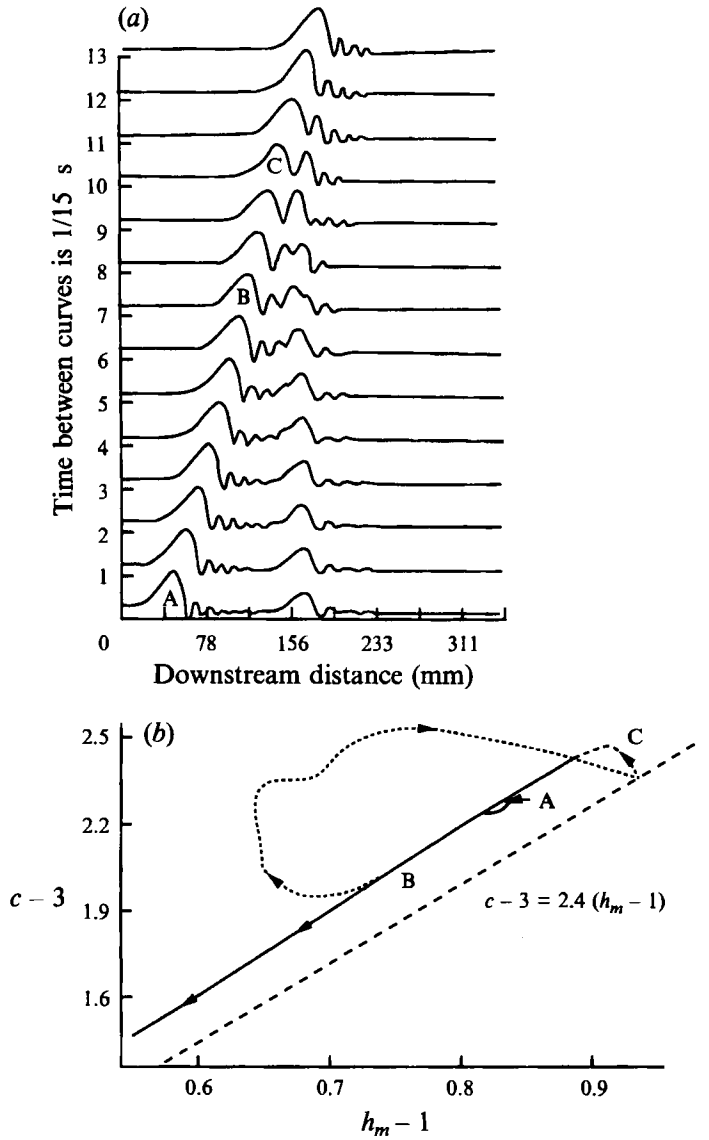

FIGURE 12. Decay dynamics of the excited back pulse and the new pulse generated by coalescence in real and dimensionless units at $\delta = 0.09$. The labels A, B and C correspond to the indicated pulse of the 'snapshots' shown. Coalescence occurs between B and C. The amplitude h_m and speed c are cross-plotted in (*b*) with the dotted line representing the short interval during coalescence. Both excited pulses decay by the same decay rate in time and when cross-plotted, lie on the same $\hat{c} - \hat{h}$ straight line which is very close to the $\hat{c} = 2.4\hat{h}$ dashed line. This verifies the quasi-steady decay through the pulse family. Note also the close encounter with two-hump transition state at 9/15 s which is represented by * in (*b*). The length and time scales for transformation to scaled variables are listed in figure 2.

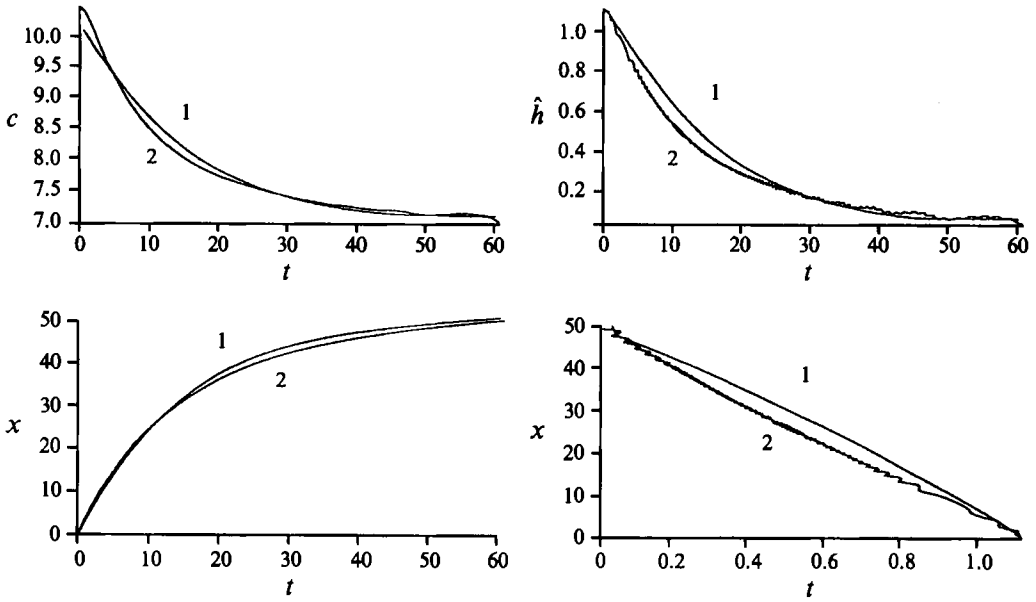

FIGURE 13. Decay dynamics of the excited pulse in figures 5 and 7 are shown as curves labelled 2. The theoretical curves 1 from the linear decay theory correspond to a decay rate of $\gamma = 0.047$.

the same substrate. Conversely, if the initial separation is less than two or three pulse widths and the back pulse is excited by the same amount, coalescence will occur but it will not be described by the present theory. In particular, the repulsion between two identical solitary pulses will most likely be masked by the dominant decaying dynamics of the back pulse during coalescence if the separation is not sufficiently far.

Having captured the decay dynamics, we proceed to study the nonlinear interaction between two pulses which does not shift the position zero mode but adds nonlinear terms to (4.2). We assume that the excited pulse has decayed sufficiently when the interaction between the two pulses becomes significant such that the interaction corresponds to two pulses on the same unit substrate. This is tantamount to assuming that the initial separation $l(0)$ is at least of the order of the characteristic decay length of an excited pulse,

$$l(0) \sim x_{\infty}. \tag{4.6}$$

If this is satisfied, the classical coherent structure theory for the interaction of two pulses on the same substrate can be derived. In this case only ψ_1 is excited and we consider a specific perturbation to a reference solitary pulse in terms of another identical solitary pulse a distance l in front. To investigate the influence of the front pulse on the back one, we expand

$$\begin{pmatrix} q \\ h \end{pmatrix}(x,t) = \begin{pmatrix} q^* \\ h^* \end{pmatrix}(x) + \begin{pmatrix} q^* \\ h^* \end{pmatrix}(x-l) - x_0(t)\psi_1(x) \tag{4.7}$$

where $\psi_1(x)$ is the position mode of the back pulse located at $x = 0$. Substituting (4.7) into the averaged equation in the frame moving with speed c^* of the two pulses, expanding to quadratic order in the mixed term between the two pulses and taking

the inner product with respect to $\varphi_1(x)$ of the back pulse, we obtain

$$\frac{dx_0}{dt} = g_f(l) = (\boldsymbol{D}, \varphi_1) \tag{4.8}$$

where $\boldsymbol{D}$ denotes the quadratic interaction terms between the two pulses in (4.7). Since the only nonlinearities of the averaged equation in the moving frame appear in the $\hat{q}$ component and not the $\hat{h}$ kinematic component, we need only be concerned with the $\hat{q}$ component of φ_1. Since the two pulses are well separated, interaction is through the tails of the two pulses and is weak. Both solitary pulses also satisfy the full steady nonlinear equation in the moving frame individually. Hence, the only interaction terms come from $\partial/\partial x(q^2/h), hh_{xxx}$ and q/h^2 in the averaged equation. Expanding to mixed terms for $q = q^*(x) + q^*(x-l)$ and $h = h^*(x) + h^*(x-l)$ and using (4) to eliminate $q^*(x)$ and $q^*(x+l)$, we obtain

$$\boldsymbol{D} = \begin{pmatrix} f \\ 0 \end{pmatrix}$$

where the scalar interaction term is a complex function of $\hat{h} = h^* - 1$:

$$f(x) = \frac{12}{5}(c^* - 1)^2 \frac{d}{dx}[\hat{h}(x)\hat{h}(x-l)] - \frac{1}{5\delta}\left[\hat{h}(x)\frac{d^3}{dx^3}\hat{h}(x-l) + \hat{h}(x-l)\frac{d^3}{dx^3}\hat{h}(x) + 2(2c^* + 3)\hat{h}(x)\hat{h}(x-l)\right]. \tag{4.9}$$

The tails described in (2.5) can be used with good accuracy to represent $h^*(x)$ and $h^*(x-l)$ in the interaction term f. In evaluating the inner product (4.8), it is important to line up the origins of φ_1 and $h^*(x)$ defined to be at the maximum of the reference pulse $h^*(x)$. Since $h^*(x-l)$ appears linearly in d and $\boldsymbol{D}$ and since the back tail of this front pulse behaves as e^{-2ml}, it is clear that the interaction force must be of the form

$$g_f(l) = -Re^{-2ml} \tag{4.10}$$

where R is only a function of the reference pulse and hence a function of δ, and $2m$ is the decay rate of the back tail of the front pulse. The explicit and only dependence on the separation l, however, is contained in the exponent. Both m and R are tabulated in table 1. Since R is positive, (4.10) indicates that the back pulse is repelled by the front one and its position is pushed to the left. Since h^* is a homoclinic orbit in the phase space of (h^*, h_x^*, h_{xx}^*), $g_f(l)$ is essentially the Melnikov function in homoclinic theory which measures how the front pulse perturbs the trajectory of the homoclinic orbit (see Balmforth *et al.* 1994, for a more detailed discussion).

The back pulse also applies a force on the front pulse and unlike $g_f(l)$ this force can be either attractive or repulsive. Let l be negative in (4.7) and let $x_1(t)\psi_1(x)$ denote the position mode of the front pulse now situated at $x = 0$. One obtains

$$\frac{dx_1}{dt} = g_b(l) = (\boldsymbol{D}, \varphi_1) \tag{4.11}$$

where $h_f(x)$ of (2.5) with the decaying oscillation is now used for $h(x-l) = h(x+|l|)$ in (4.9). The result is that the back Melnikov function is

$$g_b(l) = Se^{-ml}\cos(\beta l + \theta) \tag{4.12}$$

where S and θ are listed in table 1. We note that, owing to the oscillatory front tail of the back pulse, viz. the capillary ripples or bow waves, the interaction can push

the front pulse both forward and backward, depending on the value of l. This is consistent with earlier theories on pulse interaction (Kawahara & Toh 1988; Elphick *et al.* 1991; Chang *et al.* 1993; Balmforth *et al.* 1994).

The physical mechanism behind the attractive and repulsive forces lies in the capillary force within the ripples, which is also responsible for the unique shape of the solitary pulse. As the pulse develops and steepens owing to the pull of the gravity, a stationary pulse can only result if liquid is drained out of the pulse crest to relieve the steepening. This is provided by the first 'dimple' in front of the pulse which generates a sufficient negative capillary pressure to suck liquid out of the crest (see Wilson & Jones 1983 for a lubrication analysis of this capillary drainage mechanism). The smaller capillary waves in front of the first dimple also possess these capillary forces although their strength decays further away from the pulse as the amplitude (and curvature) diminishes. As two pulses approach each other, the back slope of the front pulse experiences a positive (negative) differential pressure in the liquid as it overlaps with a maximum (minimum) of one of the capillary waves. This elevates (depresses) the back slope of the front pulse and decreases (increases) its curvature. The generated differential capillary pressure then drains (sucks) liquid into (out of) the back half of the front pulse. This, in turn, causes the front pulse to move backwards (forwards) in a quasi-steady manner. This is why, depending on the separation between the two pulses, the front pulse can be attracted to or repelled by its neighbour.

Since $l = x_1 - x_0$, we can combine (4.8) and (4.11) to yield a dynamical equation for the separation between two pulses. If we now combine this with the linear decay dynamics of the back excited pulse, a self-contained dynamical system that describes the binary interaction between an excited back pulse and a stationary front pulse results:

$$\frac{\mathrm{d}}{\mathrm{d}t}\begin{pmatrix} l \\ \hat{\chi} \end{pmatrix} = \begin{pmatrix} 0 & -\alpha \\ 0 & -\gamma \end{pmatrix}\begin{pmatrix} l \\ \hat{\chi} \end{pmatrix} + \begin{pmatrix} g(l) \\ 0 \end{pmatrix} \tag{4.13}$$

where $g(l) = g_b(l) - g_f(l)$. This is the simple dynamical system we seek that elucidates binary interaction.

The attractive binary force generated by the oscillatory tail immediately suggests the possibility of bounded pairs and periodic pulse trains. The former corresponds to two identical pulses $\hat{\chi} = 0$ travelling in synchrony such that the separation remains constant, as seen in figure 6, while the latter corresponds to a train of equally spaced pulses. Kawahara & Toh (1988) and Elphick *et al.* (1991) have shown the existence of the former while Chang *et al.* (1993*a*) constructed the latter for falling films. Pulses travelling with identical speeds but random spacing have also been shown to be possible (Balmforth *et al.* 1994). Most of these earlier theories focused on the KS equation and its generalization which are not suitable for the coherent structure theory as we have shown. More importantly, the additional speed mode ψ_2 with amplitude $\hat{\chi}$ or $\hat{c}$ in (4.13) changes the dynamics significantly.

Coalescence is the key difference and the bounded pairs play an important role in this event. Compare for example the decay length $x_\infty(\sim 50)$ of an excited pulse after coalescence to the characteristic binary interaction length $m^{-1} \sim 5$. Without coalescence the pulses are never close enough to interact, and with coalescence only binary interaction and bounded pairs are important. The bounded pairs have separations l_i defined by $g(l_i) = 0$. As shown in the sketch of figure 14, a countable infinite number of possible l_i exists due to the particular form of the Melnikov functions g_f and g_b. This actually corresponds to a Shilnikov bifurcation from a single-loop homoclinic orbit to a double-loop one (Glendinning & Sparrow 1984).

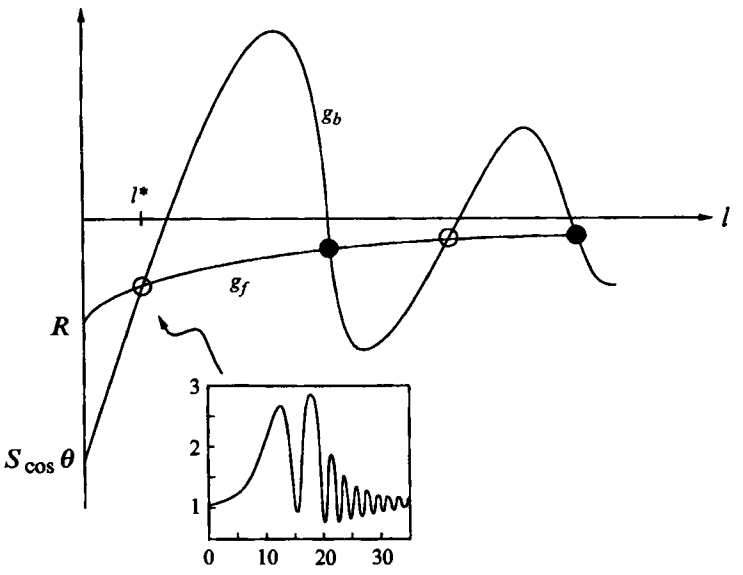

FIGURE 14. Schematic of the Melnikov functions for binary interaction. There is an infinite number of possible bounded pairs represented by the intersections. The one with the shortest separation l^* is unstable (open circles). The constructed two-hump solitary pulse corresponding to this transition state is shown in the inset.

We have numerically constructed the actual two-hump solitary waves, corresponding to the double-loop homoclinic orbit, for the averaged equations with separation l_2 and speed c_2^*. (See Chang *et al.* 1993*b*, for a clarification of how the two-hump solitary pulse family bifurcates from the one-hump family.) These two-hump solitary waves hence correspond to the shortest unstable bounded pairs estimate from the coherent structure theory here. They can be approximated by a root l^* of $g(l)$ which is unstable, $g'(l^*) > 0$. We choose l^* to be the closest unstable root of $g(l)$ to l_2. At low δ, there are typically another one or two smaller unstable roots but they are much smaller than the pulse width w and are hence meaningless. Our model then predicts that any two identical pulses on the same substrate separated by a distance less (larger) than l^* will attract (repel) each other irreversibly. The two-hump solitary pulse hence becomes a transition state for coalescence. At exactly l^*, more precisely l_2, the unstable transition state can be sustained indefinitely as in figure 6*b*. Note the resemblance of the asymptotic state in figure 6*b* to the two-hump bounded pair in figure 14. Note also that the values of l_2 and l^* are of the order of the pulse width w in table 1. The accurate estimate of l_2 by l^* is then rather surprising since the Melnikov theory should only be valid when the two pulses are further separated than l^*. We are unable to explain this coincidence. Our numerical experiments with the actual two-hump solitary waves are also consistent with those of figures 5 and 6 – slight perturbations leads to either coalescence or repulsion. The passage through the transition state represented by this unstable bounded pair with separation l^* is evident in figures 5 to 7 and figure 12. Every close encounter seems to evolve through this two-hump state regardless of whether coalescence actually takes place. It is also observed in Liu & Gollub's experimental tracings for binary interaction on an inclined film. We also note that in the repulsion case of figure 5*b* and 6*a*, the two pulses approach a stable bounded pair whose separation is larger than l^*.

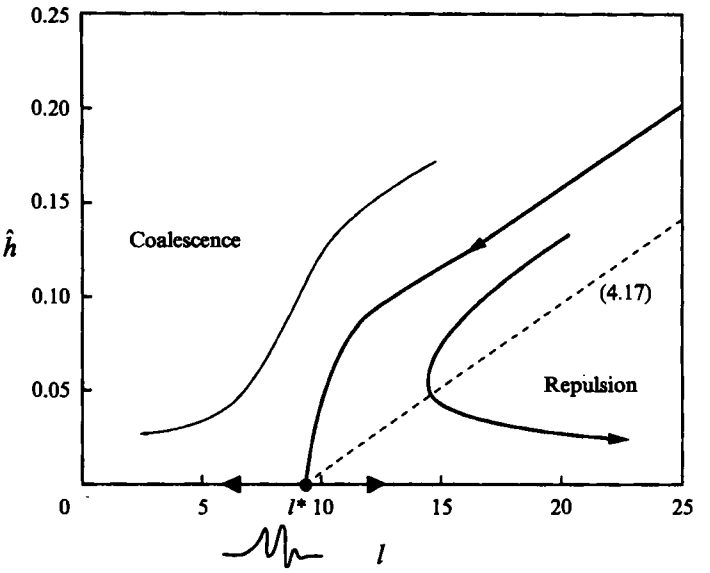

FIGURE 15. Phase-plane trajectories of dynamical system (4.14) for $\delta = 0.03$ showing the bounded-pair transition state as a saddle point and its stable manifold as a boundary for the domain of attraction of the coalescence phenomenon. Coalescence experiment with $l(0) = 25$ yields $\hat{h}_c(0) = 0.26$ which is close to the 0.21 value on the stable manifold. Approximation (4.17) which yields $\hat{h}_c(0) = 0.14$ is also shown. The deviation occurs at the inner region close to l^* where the interaction dynamics is as important as the outer decay dynamics.

It is convenient to replace $\hat{\chi}$ by $\hat{c}$ in (4.13) to yield

$$\frac{\mathrm{d}}{\mathrm{d}t}\begin{pmatrix} l \\ \hat{c} \end{pmatrix} = \begin{pmatrix} 0 & -1 \\ 0 & -\gamma \end{pmatrix}\begin{pmatrix} l \\ \hat{c} \end{pmatrix} + \begin{pmatrix} g(l) \\ 0 \end{pmatrix}. \tag{4.14}$$

The phase-space trajectory of (4.14) is shown in figure 15. It is clear that the transition state is actually a saddle point whose stable manifold demarcates initial conditions which lead to coalescence from ones that do not. These initial conditions are determined only by the initial excitation of the back pulse, as measured by $\hat{c}(0)$, and the initial separation $l(0)$. The degree of excitation of the back pulse can also be measured by $\hat{h}(0)$ and $\hat{\chi}(0)$. The numerical experiments of figures 5 and 6 then correspond to the initial condition to either side of the stable manifold and right on it. This stable manifold can be estimated by exploiting the different length scales of the long-range decay and the short-range interaction. Away from the saddle point, $\hat{c}$ and l decay as in (4.3) and (4.4), which can be combined to yield

$$\hat{c} = \hat{c}(0) + \gamma(l - l(0)). \tag{4.15}$$

This is a good approximation of the long-range dynamics except within a small neighbourhood of the saddle point when the short-range forces in $g(l)$ become important. However, since $l(0) \gg l^*$ and $\hat{c}(0) \gg 0$, it is a good approximation to assume that (4.15) goes through the saddle point to obtain an estimate of the stable manifold and hence a condition for coalescence:

$$\hat{c}(0) = \gamma(l(0) - l^*). \tag{4.16}$$

Converting to $\hat{h}(0)$ by the correlation $\hat{c} = 2.4\hat{h}$ discussed earlier, we get

$$\hat{h}(0) = \frac{\gamma}{2.4}(l(0) - l^*). \tag{4.17}$$

This then represents an estimate of the critical separation $l(0)$ for coalescence for a binary pair whose back excited pulse has a degree of excitation of $\hat{h}(0)$.

As seen in figure 15, it represents a good estimate of the stable manifold although $\hat{h}(0)$ is underpredicted owing to the inner region near the transition-state saddle point. We have carried out a series of numerical experiments with a stationary pulse in front and an excited pulse at exactly $l(0) = 25$ units behind it. The excited pulse has an incremental amplitude over the stationary pulse of $\hat{h}(0)$. We adjust this $\hat{h}(0)$ until a critical excitation is found which demarcates coalescence from repulsion. The measured critical values of $\hat{h}_c(0)$ are compared to the predicted one of (4.17) in table 1. Without including the slow dynamics of the non-zero eigenvalue in figure 11, we do not expect our theory based on the two perturbed zero modes to be accurate for $\delta < 0.03$. For $\delta > 0.03$, however, the theory is of the same magnitude as the exact value, which is quite acceptable considering the approximations made. In fact, criterion (4.17) should break down when the interaction parameters R and S become large since the inner region shown in figure 15 then becomes significant. However, as seen in table 1, while the prediction improves at small δ where R and S are small, it remains quite acceptable at larger δ values, given that (4.17) typically underpredicts as shown in figure 15.

5. Discussion

Although we have constructed a theory for binary interaction, application of the theory to the multi-pulse system of figure 1 still requires some work. The theory was developed by using the pulse on a unit substrate as a reference. The pulses in figure 1 lie on substrates much smaller than unity and a change of reference pulse to recalculate the coefficients in table 1 must be done with the help of transformation (3.4). More difficult, however, is the estimate of the degree of excitation due to coalescence. One approach is to find a pulse with double the mass and use the difference in amplitude between this larger pulse and the original pulses before interaction as a measure of excitability $\hat{h}(0)$. The asymptotic behaviour of the pulse dynamics at large δ shown in table 1 may allow us to develop a completely analytical description of the equilibrium separation and the evolution towards this equilibrium seen in figure 2. This asymptote must, of course, be recalibrated for different reference pulses but even the calibration may benefit from an analytical elucidation of the asymptotic behaviour at large δ. We note that the coalesced mass does not resemble a solitary pulse initially but it decays rapidly, with a decay rate measured by the stable point eigenvalue shown in figure 11, such that a solitary pulse emerges soon afterwards. This is shown in figure 12 where the amplitude of a pulse generated by coalescence is seen to approach the slow γ decay of a solitary pulse within 3 units of time. This is compared to the slow exponential decay of an excited pulse which takes about 20 to 50 units as measured by γ^{-1}. This suggests that the coalescence event can be considered instantaneous in the theory for the full dynamics. Finally, the ad hoc manipulation of the inner products to estimate γ should be carried out more rigorously by including the continuous spectrum.

This work is supported by DOE under the Engineering Research Program.

Appendix. The adjoint eigenvalue problem

Using the L_2 inner product,

$$(\boldsymbol{u}, \boldsymbol{v}) = \int_{-\infty}^{\infty} (u_1 v_1 + u_2 v_2) \mathrm{d}x.$$

the adjoint operator to $\boldsymbol{L}$ of (6) is defined as

$$(\boldsymbol{u}, \boldsymbol{L}\boldsymbol{v}) = (\boldsymbol{L}^{\dagger}\boldsymbol{u}, \boldsymbol{v})$$

After standard integration by parts and index change, the adjoint operator is found to be

$$\boldsymbol{L}^{\dagger} = \begin{pmatrix} \mathrm{L}_1^{\dagger} & \dfrac{\mathrm{d}}{\mathrm{d}x} \\ \mathrm{L}_2^{\dagger} & -c\dfrac{\mathrm{d}}{\mathrm{d}x} \end{pmatrix}$$

where

$$\mathrm{L}_1^{\dagger} = -c\frac{\mathrm{d}}{\mathrm{d}x} + \frac{12}{5}\frac{q^*}{h^*}\frac{\mathrm{d}}{\mathrm{d}x} - \frac{1}{5\delta}\frac{1}{(h^*)^2}\cdot,$$

$$\mathrm{L}_2^{\dagger} = -\frac{6}{5}\left(\frac{q^*}{h^*}\right)^2\frac{\mathrm{d}}{\mathrm{d}x} + \frac{1}{5\delta}\left[\frac{\mathrm{d}^3 h^*}{\mathrm{d}x^3} + 1 + \frac{2q^*}{(h^*)^3}\right]\cdot - \frac{1}{5\delta}\frac{\mathrm{d}^3}{\mathrm{d}x^3}[h^*\cdot]$$

with the same bounded boundary conditions as the eigenvalue problem (3.1). It is quite obvious that a null eigenfunction of the adjoint operator $L^{\dagger}$ is

$$\boldsymbol{\varphi}_2 = \begin{pmatrix} 0 \\ d \end{pmatrix}$$

where d is a constant. Another null eigenfunction L_1 was found numerically whose first component φ_1^1 goes to zero at the infinities but its second component φ_1^2 approaches -1 at $-\infty$ and $+1$ at $+\infty$. This null eigenfunction is shown in figure 10.

REFERENCES

Balmforth, N. J., Ierley, G. R. & Spiegel, E. A. 1994 Chaotic pulse trains. *SIAM J. Appl. Maths* **54**, 1291–1304.

Chang, H.-C. 1986 Traveling waves on fluid interfaces: normal form analysis of the Kuramoto-Sivashinsky equation. *Phys. Fluids* **29**, 3142–3147.

Chang, H.-C. 1994 Wave evolution on a falling film. *Ann. Rev. Fluid Mech.* **26**, 103–136.

Chang, H.-C., Cheng, M., Demekhin, E. A. & Kopelevich, D. I. 1994 Secondary and tertiary excitation of three-dimensional patterns on a falling film. *J. Fluid Mech.* **270**, 251–275.

Chang, H.-C., Demekhin, E. A. & Kopelevich, D. I. 1993*a* Nonlinear evolution of waves on a vertically falling film. *J. Fluid Mech.* **250**, 433–480.

Chang, H.-C., Demekhin, E. A. & Kopelevich, D. I. 1993*b* Laminarizing effects of dispersion in an active-dissipative nonlinear medium. *Physica* D **63**, 299–320.

Cheng, M. & Chang, H.-C. 1995 Competition between sideband and subharmonic secondary instability on a falling film. *Phys. Fluids* **7**, 34–54.

Demekhin, E. A., Kaplan, M. A. & Shkadov, V. Ya. 1987 Mathematical models of the theory of viscous liquid films. *Izv. Akad. Nauk SSSR Mekh. Zhidk. i Gaza* **6**, 73–81.

Demekhin, E. A. & Shkadov, V. Ya. 1985 Two-dimensional wave regimes of thin liquid films. *Izv. Akad. Nauk SSSR. Mekh. Zhidk. i Gaza* **3**, 63–97.

Demekhin, E. A. & Shkadov, V. Ya. 1986 Theory of solitons in systems with dissipation. *Izv. Akad. Nauk SSSR. Mekh. Zhidk. i Gaza* **3**, 91–97.

Elphick, C., Ierley, G. R., Regev, O. & Spiegel, E. A. 1991 Interacting localized structures with Galilean invariance. *Phys. Rev.* A **44**, 1110–1122.

FRISCH, U., ZHEN, S. S. & THUAL, O. 1986 Viscoelastic behaviour of cellur solutions to the Kuramoto-Sivashinsky model. *J. Fluid Mech.* **168**, 221–240.

GLENDINNING, P. & SPARROW, C. T. 1984 Local and global behaviour near homoclinic orbits. *J. Statist. Phys.* **35**, 645–696.

JAYAPRAKASH, C., HAYOT, F. & PANDIT, R. 1993 Universal properties of the two-dimensional Kuramoto–Sivashinsky equation. *Phys. Rev. Lett.* **71**, 12–15.

KALLIADASIS, S. & CHANG, H.-C. 1994 Drop formation during coating of vertical fibres. *J. Fluid Mech.* **261**, 135–168.

KAWAHARA, T. & TOH, S. 1988 Pulse interaction in an unstable-dissipative nonlinear system. *Phys. Fluids* **31**, 2103–2111.

LIU, J. & GOLLUB, J. P. 1993 Onset of spatially chaotic waves on a falling film. *Phys. Rev. Lett.* **70**, 2289–2292.

LIU, J. & GOLLUB, J. P. 1994 Solitary wave dynamics of film flows. *Phys. Fluids* **6**, 1702–1712.

NAKAYA, C. 1989 Waves on a viscous fluid film down a vertical wall. *Phys. Fluids* A **1**, 1143–1154.

PROKOPIOU, Th., CHENG, M. & CHANG, H.-C. 1991 Long waves on inclined films at high Reynolds number. *J. Fluid Mech.* **222**, 665–691.

PUMIR, A., MANNEVILLE, P. & POMEAU, Y. 1983 On solitary waves running down an inclined plane. *J. Fluid Mech.* **135**, 27–50.

SALAMON, T. R., ARMSTRONG, R. C. & BROWN, R. A. 1994 Traveling waves on inclined films: numerical analysis by the finite element method. *Phys. Fluids* **6**, 2202–2220.

SHKADOV, V. Ya. 1967 Wave conditions in the flow of thin layer of a viscous liquid under the action of gravity. *Izv. Akad. Nauk. SSSR Mekh. Zhidk. i Gaza* **1**, 43–50.

STAINTHORP, F. P. & ALLEN, J. M. 1965 The development of ripples on the surface of a liquid film flowing inside a vertical tub. *Trans. Inst. Chem. Engrs* **43**, 85–91.

WILSON, S. D. R. & JONES, A. F. 1983 The entry of a falling film into a pool and the air-entrainment problem. *J. Fluid Mech.* **128**, 219–230.